

**NANO THERMAL AND CONTACT POTENTIAL ANALYSIS
WITH HEATED PROBE TIPS**

A Thesis Presented to

The Academic Faculty

By

Jessica Lynn Remmert

In Partial Fulfillment of the Requirements for the Degree

Master of Science in Mechanical Engineering

Georgia Institute of Technology

May 2007

**NANO THERMAL AND CONTACT POTENTIAL ANALYSIS
WITH HEATED PROBE TIPS**

Approved:

Dr. William P. King, Chair
Mechanical Engineering
Georgia Institute of Technology

Dr. Samuel Graham
Mechanical Engineering
Georgia Institute of Technology

Dr. Clifford Henderson
Chemical and Biomolecular Engineering
Georgia Institute of Technology

Date Approved: April 2, 2007

ACKNOWLEDGEMENTS

I would like to thank my advisor, Dr. William King, for the opportunity to learn about atomic force microscopy and for his guidance on experimental work and results. I am also grateful that I have had the opportunity to work with and learn from Dr. Yan Wu and the members of the Nanoscale Thermal Processing Lab at Georgia Institute of Technology and the University of Illinois.

TABLE OF CONTENTS

ACKNOWLEDGEMENTS.....	iii
LIST OF TABLES.....	v
LIST OF FIGURES.....	vi
SUMMARY.....	viii
CHAPTER 1: INTRODUCTION.....	1
CHAPTER 2: THERMAL ANALYSIS WITH A HEATED PROBE.....	5
2.1 Previous Work.....	5
2.2 Sample Preparation.....	6
2.3 Calibration Methods.....	7
2.4 Experimental Method.....	11
2.5 Thermal Analysis of HDPE.....	13
2.6 Thermal Analysis of Acetylsalicylic Acid.....	17
2.7 Results and Discussion.....	19
2.8 Thermally Induced Bending.....	26
CHAPTER 3: FEASIBILITY EXPERIMENT WITH A HEATED KELVIN PROBE.....	29
3.1 Experimental Method.....	29
3.2 Analytical Approach.....	34
3.2.1 Contact Potential Measurement.....	34
3.2.2 Seebeck Coefficient.....	37
3.2.3 Electrostatic Force.....	39
3.2.4 Space Charge Effect.....	39
3.3 Results and Discussion.....	40
CHAPTER 4: CONCLUSIONS AND FUTURE WORK.....	49
REFERENCES.....	52

LIST OF TABLES

Table 1. Seebeck Coefficients for Doped Silicon [V/K].....	38
Table 2. Thermal Voltages [V].....	38

LIST OF FIGURES

Figure 1. SEM of Type II heated probe.....	7
Figure 2. Circuit diagram.....	8
Figure 3. Calibration curves.....	10
Figure 4. AFM feedback control monitoring displacement of tip relative to surface.....	12
Figure 5. Displacement of the tip at the softening point of HDPE.....	14
Figure 6. Tip displacement and resistance change for HDPE.....	15
Figure 7. Indents formed by an in-contact temperature ramp on HDPE.....	16
Figure 8. Tip displacement and resistance change for aspirin.....	18
Figure 9. Indents formed by an in-contact temperature ramp on aspirin.....	18
Figure 10. Average temperature transitions and indentation depths for HDPE as a function of contact force.....	19
Figure 11. Observed temperature transitions and indentation depths for aspirin..	20
Figure 12. HDPE transitions as a function of contact force.....	22
Figure 13. Resistance change at each of the observed HDPE transitions.....	22
Figure 14. Extracted LVDT signal on glass for various contact forces.....	27
Figure 15. Heat-induced bending.....	28
Figure 16. Circuit diagram for the case in which the tip is both unheated and biased.....	30
Figure 17. Circuit diagram for the case in which the tip is heated but unbiased...	31
Figure 18. Circuit diagram for the case in which tip is both heated and biased...	31
Figure 19. Force-distance measurement.....	33
Figure 20. Example raw deflection – LVDT output.....	33
Figure 21. Heated Kelvin probe.....	35

Figure 22. Possible surface charges states on the silicon top.....	40
Figure 23. Example force-distance plot in which both tip bias and temperature are varied.....	42
Figure 24. Normalized result 100 nm from contact.....	42
Figure 25. Observed contact potential shift 100 nm from contact for various tip biases and a probe temperature of approximately 200°C.....	43
Figure 26. Measured contact potential as a function of distance.....	44
Figure 27. Effect of temperature on measured contact potential 100 nm from contact.....	46
Figure 28. Effect of temperature on unbiased tip.....	46

SUMMARY

This thesis describes two closed-loop AFM methods that rely on a heated silicon probe to interrogate a surface. The first method identifies the softening temperatures of a selected polymer and organic substrate as a function of contact force and surface hardness. In the second method, the cantilever is implemented as a Kelvin probe to study the effect of temperature on the measured contact potential. Both experiments examine the interaction between the tip and substrate and analyze sample effects both induced and sensed by the probe.

CHAPTER 1

INTRODUCTION

Atomic force microscopy (AFM) enables three-dimensional mapping and characterization of substrates with nanometer scale resolution. The technique is based on the controlled-force operation of a sharp cantilever tip at a sample surface. With feedback activated, the instrument monitors cantilever deflection to gauge the interaction between tip and sample and adjust the separation distance accordingly [1]. Beyond visualizing surfaces, AFM cantilevers can be designed to probe subsurface material [2, 3] or induce measurable topographic changes [4]. This work pertains to use of the silicon cantilever, which can act as a thermal source or electrical stimulus to target specific material properties. The experiments described in this thesis demonstrate the versatility of the heated probe and consider its use in AFM and related technologies.

In scanning mode, the heated cantilever can distinguish features and material phases by physically contacting the surface and/or by sensing changes in the dissipated power. This is utilized in scanning thermal probe microscopy (SThM) to isothermally map surfaces based on variations in the thermal conductivity or specific heat capacity [5], and in part motivates the experiments described in Chapter 2. Alternately, a mechanically oscillating probe can read topography at fixed distance under an applied electrostatic field. The voltage that is required to null the cantilever vibrations is a measure of the contact potential and is used to generate electrical maps via scanning Kelvin probe microscopy (SKPM). Chapter 3 assesses the combined influence of temperature and potential on the force interaction between the tip and a conducting substrate in a basic KPM measurement. Common to both experiments is the cantilever's

ability to heat under electrical excitation. Both also rely on the force feedback to track the tip height relative to the surface. The first experiment additionally utilizes the probe's temperature sensing capabilities, while the second extracts information from the monitored deflection.

Chapter 2 describes an experiment in which the cantilever temperature was ramped with the tip engaged on the surface. Tip displacement was continually tracked during indent formation with simultaneous measurement of heat loss by monitoring the probe's electrical resistance. The objective is to determine the softening point of a selected polymer and pharmaceutical analyte by localized thermal analysis (LTA). Motivation partly stems from nanosampling, which requires knowledge of phase-specific thermal responses to identify and extract mass from multicomponent systems. The sample response has previously been shown to vary with the choice of probe [5]. In addition, efforts have been made to distinguish between the onset of softening and material phase transitions [6, 7]. It is therefore important to address the factors that can influence interpretation of the transition temperature. Chapter 2 compares the thermal responses of two substrates that differ in surface hardness. The contact force was varied on each to ascertain its influence on heat dissipation to the substrate with continued submersion of the tip.

While previous LTA studies have identified distinct transitions comparable to values acquired by bulk heating [8], others have observed significant deviations [9, 10]. A suggested cause for the discrepancy is the contact resistance at the tip-sample interface, which is modulated by tip pressure and is on the order of 10^7 K/W. Two factors may affect contact resistance as the indent is formed: (1) as the probe stiffness decreases with

temperature, force also decreases at constant deflection, and (2) the contact area increases due to local softening. Since the two effects counteract one another and are difficult to isolate during a temperature ramp, other experiments must be designed to measure them. Chapter 2 considers a few methods which aim to characterize thermally induced deflection that can detract from tip displacement. Although cantilever stiffness and bending contribute to the measured responses, the effects are expected to be less significant than the interaction between tip and sample. The experiment addresses the second factor by varying the initial contact force. This also has important implications for the thermal images obtained via SThM. As the tip scans, surface roughness can change the contact area and affect the measured conductivities [11]. This method means to study the effect of the changing contact area on the material softening rate, and could perhaps decouple the heat loss associated with a softening substrate and that reflecting variations in chemical composition.

Chapter 3 describes a feasibility experiment in which the attractive force between the semiconducting tip and a charged conducting film is studied as the tip approaches the sample from a distance. A number of factors are considered which determine the strength of the electrostatic field between the two electrodes. These include the driving and thermal voltages, work function difference, surface potential, space charge, and long-range background forces. Various circuits were assembled to test combinations of applied heat and bias. Since the aim is to quantify the effect of heat on the measured contact potential, the Seebeck coefficient was further estimated for various temperatures and doping profiles. This experiment is primarily motivated by SKPM applications, such as surface potential mapping, in which subsurface particles or phases are identified by

their contrasting native voltages. In particular, SPKM has been used to probe grain boundaries [12] and diagnose corrosion in electronic devices [13]. It can also induce and detect trapped surface charges and has potential applications in data storage and self assembly processes [14].

Standard Kelvin probes have lateral resolution on the order of 100 μm [3]. The enhanced spatial resolution of the silicon tip and its ability to conduct heat therefore suggest it is a promising tool for SKPM applications. Research has identified the thermoelectric effect introduced by the probe tip as a means to profile dopant diffusion in semiconducting devices [15, 16]. The heated tip is also suited to characterize contact resistance at junctions in small-scale electronic devices. Previous studies that have assessed limitations arising from reduced contact area or increased current have relied on the four-terminal Kelvin probe to measure the Seebeck effect [17]. The heated probe offers a model for the silicon-metal interface with the further advantage of independently monitoring a localized temperature gradient.

The experiments described in this work employ the heated cantilever to characterize materials based on their inherent thermal and electrical properties. Homogeneous samples were selected so that other factors could be varied, such as the applied contact force or the applied bias. These methods provide the basis for and may be used in conjunction with nondestructive AFM scanning techniques. This work could therefore be extended to characterize multiphase materials for various applications as described above.

CHAPTER 2

THERMAL ANALYSIS WITH A HEATED PROBE

The heated probe has been implemented in localized thermal analysis (LMA) of polymer films and organic analytes to measure surface thermal responses more accurately than can be achieved by uniform sample heating. By bringing the probe in contact with the substrate, it can induce surface phase transitions and simultaneously sense the associated increase in absorbed energy. Atomic force microscopy allows tip displacement to be monitored during indent formation. These two measures can independently identify the onset of softening by various AFM techniques, including heated force-distance measurements and constant-contact temperature ramps, which vary in their sensitivity to the applied contact force.

2.1 Previous Work

Two methods that assess softening by AFM feedback control are briefly compared here: the first evaluates the surface response with the tip engaged during a temperature ramp, while the second isothermally measures interaction while approaching the substrate from a distance. The initial contact force is of greater importance in the first method due to the extended dwell time leading up to the transition. For the heated force-distance method, the penetration depth is determined not only by the pre-established force, but also the approach velocity, which governs heat dissipation in conjunction with the changing thermal impedance. The force-distance method therefore provides a better initial estimate of surface compactness as a function of temperature, and avoids prolonged contact with the subsurface material which may over-deflect the probe and result in less accurate height tracking with continued submersion of the tip. On the other

hand, it requires a range of isothermal approaches and rates to identify the softening point, whereas the constant-contact method continues to capture information about the sinking tip as the temperature is ramped. In this study, we rely on the former method but simultaneously vary the force to assess its impact on the transition. Material hardness also affects the observed transitions. For instance, a stiff surface displays clear, heat-induced transitions, whereas a softer one will respond in part to the weight of the probe.

2.2 Sample Preparation

Two substrates with comparable bulk melting temperatures but dissimilar surface rigidity were tested: high density polyethylene (HDPE) and acetylsalicylic acid (aspirin). The HDPE sample was cross-sectioned from an extruded rod and embossed under 500 lbs of pressure at a plate temperature of 100 °C for approximately 5 minutes. The polymer was compressed under heat to reduce surface asperity and facilitate subsequent indentations formed by the tip. The expected melting temperature of 135 °C was not exceeded during the embossing step in order to preserve chemical integrity. The aspirin sample was prepared by holding 99+% Sigma-Aldrich powder (CAS 50-78-2) ten degrees above the melting temperature of 134-136 °C for 2 minutes. Melting the aspirin between coverslips reduced contamination and yielded an even surface that was sufficiently solid for indentation.

2.3 Calibration Methods

All experiments were performed with an Asylum MFP 3D Atomic Force Microscope and phosphorous-doped silicon cantilevers fabricated by the silicon-on-insulator process. Fabrication and characterization of the heated probes has been thoroughly described by Lee et al. [18]. The specific geometry of the probes employed here includes a triangular free end that was lightly doped to 10^{17} cm^{-3} to achieve resistive heating under passing current. Inner and outer lengths of the heated bridge are 107 and 173 μm , respectively, while the legs span 670 μm and are mounted to the conductive silicon chip via 750 μm anchors [Figure 1]. Dopant concentration in the legs is comparatively greater (10^{20} cm^{-3}) such that heat generation is essentially a free-end effect.

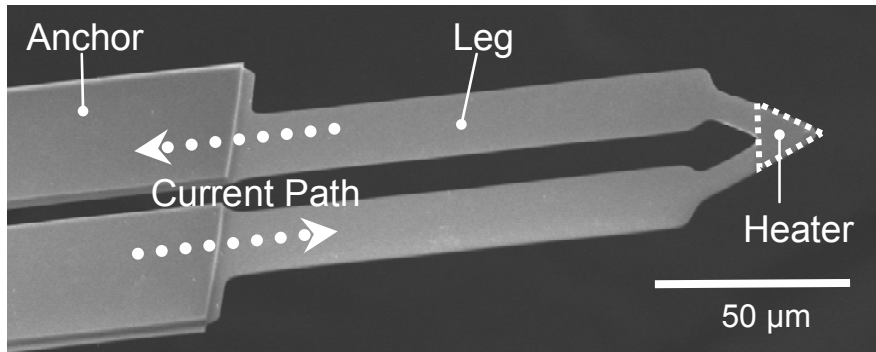


Figure 1. SEM of Type II heated probe. Cantilevers were batch-fabricated by the silicon-on-insulator process at Georgia Tech. Repeated isotropic plasma etching honed the tip radius to approximately 50 nm.

A standard AFM holder was modified to allow electrical contact with the probes. The probes were characterized in series with a 9.8 k Ω carbon sense resistor using a DC power supply [Figure 2]. A model 2400 Keithley sourcemeter elevated the circuit to the designated threshold voltage in 0.1 V increments at a rate of 0.08 mV/s. The threshold

voltage was identified as the thermal runaway point and predicted a drop in resistance with continued rise in power due to enhanced carrier mobility along the current path in the bridge. The circuit was immediately stepped down at the same rate after reaching peak temperature to prevent further release of intrinsic carriers [19]. The voltage across the sense resistor was measured by an Agilent 33401A multimeter and recorded concurrently with the elapsed time, source voltage, and current read by the sourcemeter. The power dissipated by the cantilever in the AFM head when removed several millimeters from the substrate was directly calculated from these values and matched against the Raman-calibrated heater temperature.

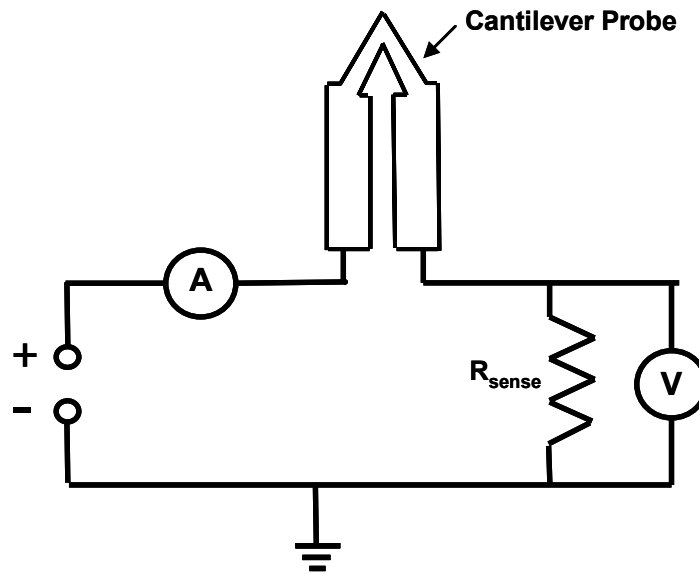


Figure 2. Circuit diagram. The elapsed time, current, and voltage drop across the 9.8 k Ω sense resistor are recorded as voltage is stepped to the circuit.

An identical circuit was assembled on the microscope stage of a Renishaw InVia Raman System. At each voltage sourced, the cantilever reached steady state under an Ar⁺ laser at 50X objective and cross-hairs were monitored closely for position within the heater region just below the tip. Laser power was set at 5% with a 60 second acquisition

count of inelastically scattered photons to obtain the Stokes peak. A Gaussian fit of the spectra identified the peak position ω was used to estimate temperature:

$$T = \frac{(\omega - \omega_o)}{A} + T_o$$

The Raman shift/cm is therefore relative to a reference peak position ω_o (typically 520 cm^{-1}) corresponding to reference temperature T_o (23 °C) and precalibrated constant A (-0.0212). The peak shifts towards lower wavenumbers with increasing temperature due to a changing interaction between bombarding phonons and the vibrating crystalline lattice [20]. It should be noted that temperature calibration based on the shifting Stokes peak is not independent of intrinsic material stress.

Barring humidity and ambient temperature fluctuations which affect device performance, the probe temperature may at any time be extracted from the Raman calibrated fit, providing that power was measured far (several mm) from the substrate. The probe used to extract the above data for HDPE and aspirin demonstrated a linear temperature-power fit below approximately 3 mW. The corresponding resistance-temperature fit may then be used to ascertain temperature with the tip engaged. In close proximity to the surface, reduced thermal impedance significantly lowers the measured resistance. It was additionally determined that the Raman Ar^+ laser and SLD in the AFM head have minimal effect on the temperature ramp of the heated probes. Calibration curves are provided in Figure 3.

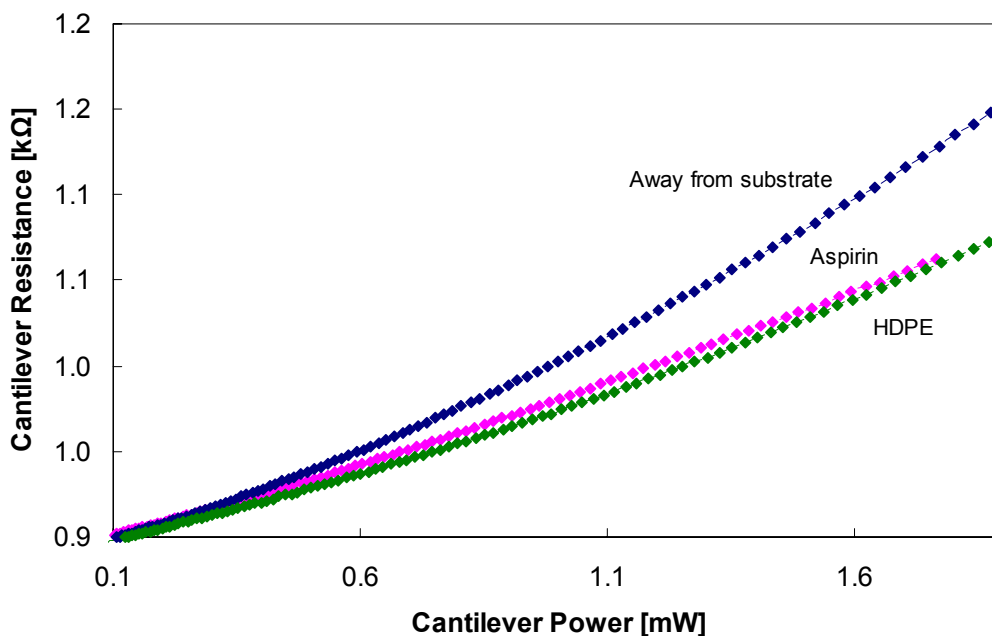
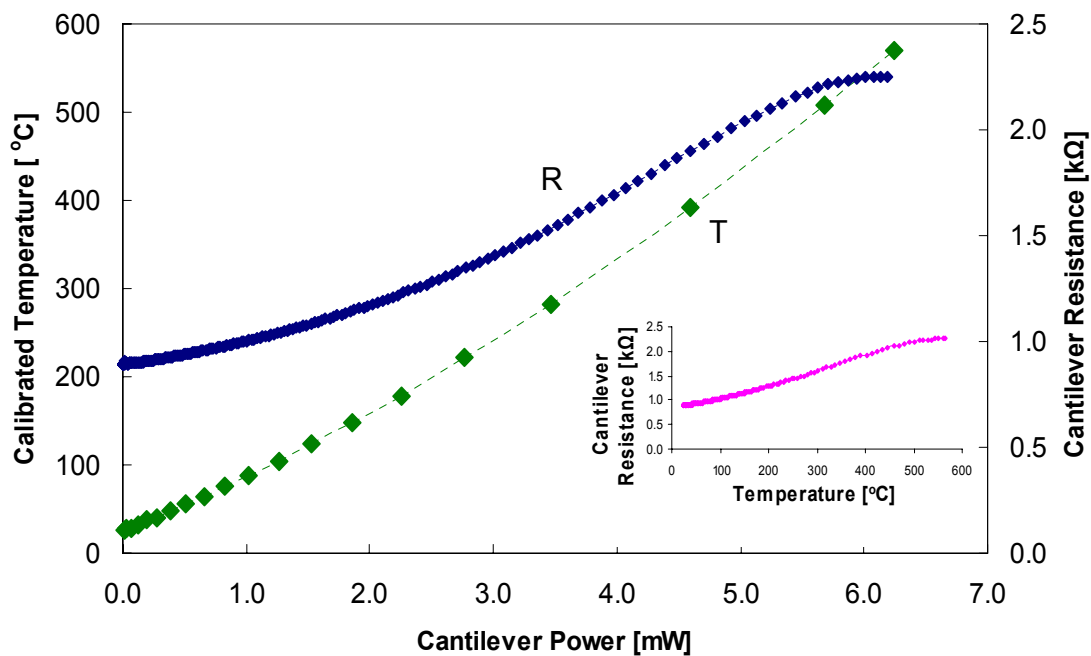


Figure 3. Calibration curves. The heater temperature is calibrated by the shifting Stokes peak method via Raman spectroscopy. Temperature is matched to the measured resistance in contact with the substrate by the power-temperature and corresponding resistance-temperature fits at ambient conditions (when the probe is far from interaction with the substrate).

Prior to indenting, cantilevers were calibrated within the MFP 3D Igor Pro software to characterize stiffness and sensitivity within the feedback control. The slope of the contact region during a force-distance measurement relates the physical deflection of the cantilever per voltage output from the photodiode. This parameter (the invOLS) is highly sensitive to the projected laser spot and total amount of light incident on the detector. It is also used to calculate the spring constant via the thermal noise method [21], during which the resonance frequency of the probe is found by vibrating a small piezo within the holder. The spring constant, optical-lever sensitivity, and observed free position vertical deflection relative to the set point value are used to calculate the applied contact force.

2.4 Experimental Method

The probes were engaged on the surface and scanned in contact mode to characterize the local topography. Indentations were formed by offsetting the tip to a specified location and establishing set point force before heating. The probe was often scanned between runs to image the resulting marks. The same probe was used to extract the data for HDPE and aspirin that follows, though the trends were shown to be repeatable with probes of different geometry.

With feedback activated, cantilever deflection is manifest within the linear variable differential transformer (LVDT) sensor output. The LVDT operates in parallel with the piezo stack and is sensitive to extension or retraction of the flexure stage that encases the optical feedback components and controls vertical displacement of the probe. A superluminescent diode incident on the cantilever legs and sensitive to their deflection is reflected onto a split photodiode, yielding a voltage output proportional to the distance

2.5 Thermal Analysis of High Density Polyethylene

The experiments described here pertain to a heated silicon probe in closed-loop AFM contact with the HDPE substrate subject to ambient conditions. The probe bends under thermal stress at elevated temperatures and, in accordance with the feedback constraint, deflects relative to the surface on which it is engaged. It also bends as a result of material expansion [5]. However, when heat is sufficiently dissipated by the probe such that the softening temperature of the substrate is approached, the tip will move into closer contact just prior to perforating the surface. The onset of penetration is suggested by a brief decrease in temperature that may coincide with increased contact between the tip and enveloping subsurface material. The thermal impedance between tip and sample is diminished as a result; equilibrium is restored upon further penetration of the tip until the threshold voltage is sourced. As shown in Figure 5, noteworthy events include initial displacement of the tip towards the surface, the onset of penetration marked by a sudden drop in probe resistance, and the final temperature escalation before power is reduced to the circuit.

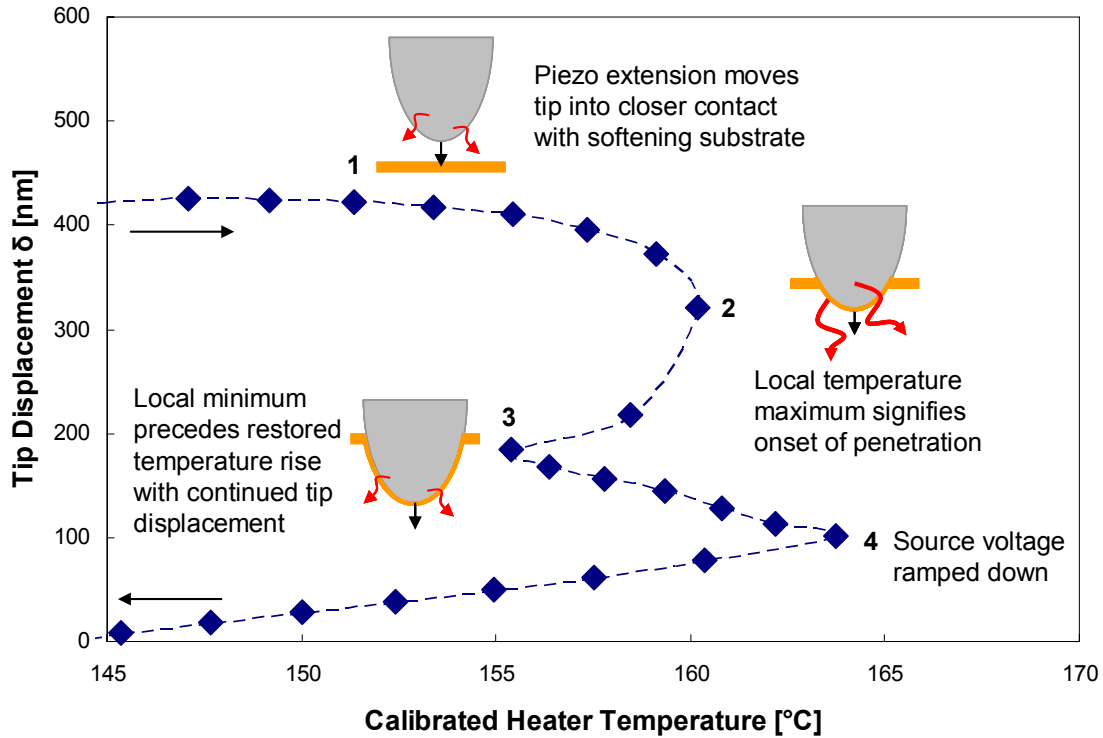


Figure 5. Displacement of the tip at the softening point of HDPE. Transitions 1-3 illustrate how the probe temperature varies as the tip sinks into the substrate. Point 4 is the maximum temperature attained before power is reduced to the circuit. The tip continues to sink as the probe cools.

The probe continues to sink as heat flows into the substrate until the temperature gradient declines to a point that the surrounding material can solidify and counteract tip pressure. The rate at which the tip penetrates into a given material is a function of the temperature ramp, surface contact area, and material thermal properties. Determination of the localized melting point is regulated by these parameters. In this investigation, a constant heating rate was maintained while the force was varied between indentations. Increasing the applied force enhances contact area and is expected to bolster heat transfer from the tip and achieve earlier onset of the downward displacement. Vertical motion of the tip depends upon the designated set point force. During thermal analysis, the probe was not operated in scanning mode but rather held stationary; lateral motion of the tip is

expected to minimally contribute to the indentations formed and corresponding height information. A typical displacement signal and measured resistance change for HDPE are provided in Figure 6. Figure 7 is an AFM image of indents formed on HDPE by thermal analysis as a function of temperature and set point force.

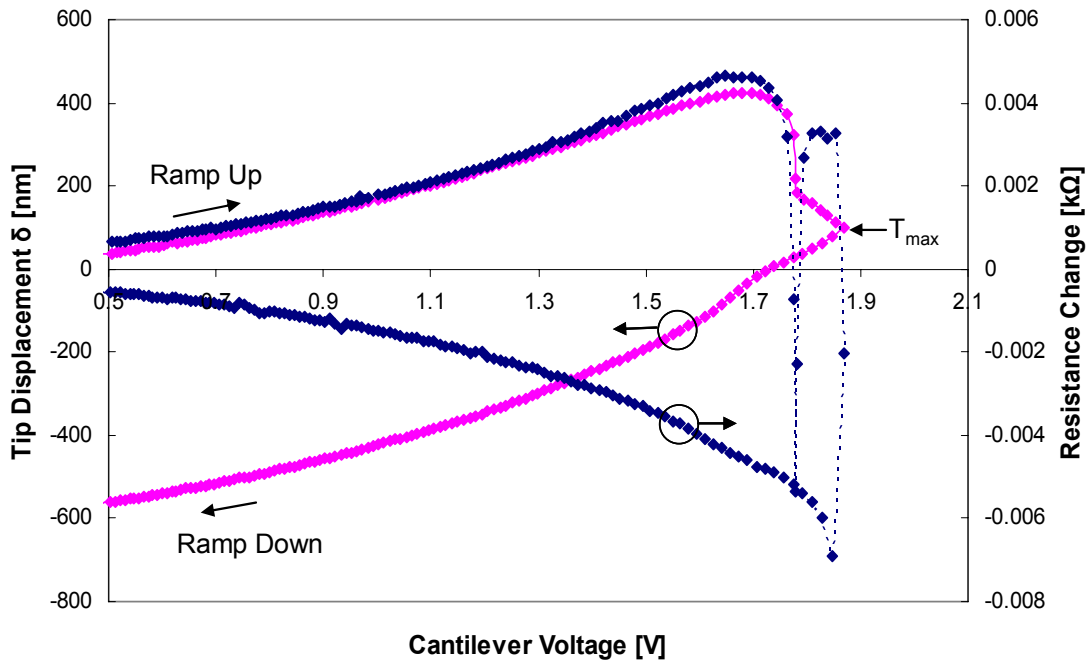


Figure 6. Tip displacement and resistance change for HDPE at 45.4 nN applied contact force. Probe resistance increases as the voltage is ramped. The probe deflects due to thermal bending and material expansion, causing the piezo to retract the tip from the surface. The onset of penetration is given by a drop in resistance that coincides with downward tip displacement. The rate of tip displacement decreases as thermal equilibrium is restored. As the probe cools, resistance increases and the tip continues to sink into the substrate.

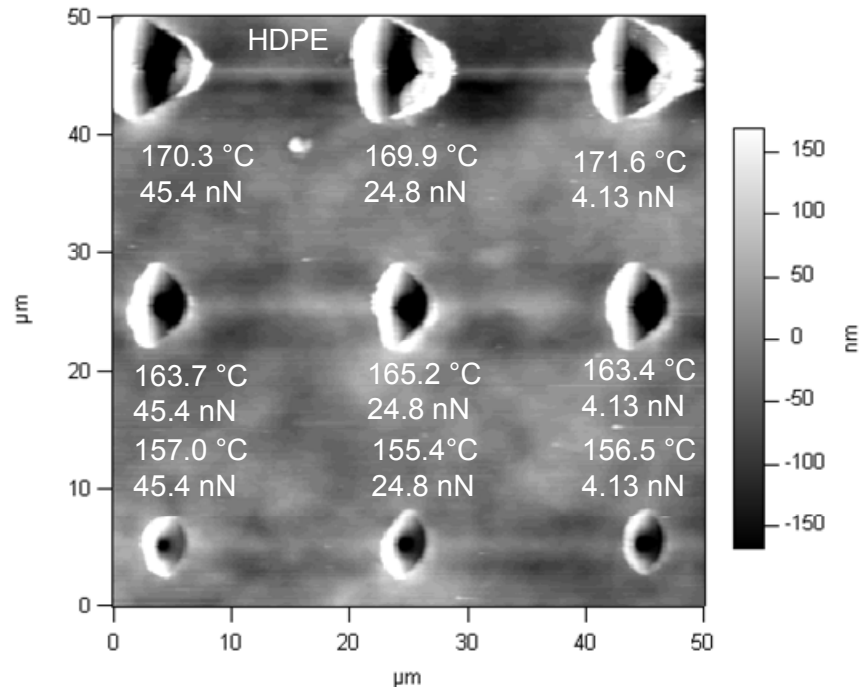


Figure 7. Indents formed by an in-contact temperature ramp on HDPE. Both the maximum temperature and applied contact force were varied; heating and cooling rates were held constant.

2.6 Thermal Analysis of Acetylsalicylic Acid

In contrast to the sharp transitions observed for HDPE, the onset of aspirin softening is apparent by a gradual extension of the piezo that reverses the initial upward tip displacement associated with bending and material expansion. A typical result is shown in Figure 8. Continuous sinking of the tip is suggested by the moderate slope between maximum upward displacement and threshold voltage. As indicated by the resistance change, up to 1.3 V heat loss is relatively steady and uninterrupted by an abrupt increase in contact area. However, the resistance change often starts to fluctuate around this value (corresponding to a temperature of approximately 100 °C) and does not stabilize until approximately 90 °C on the ramp down. While this trend precludes identification of specific temperature transitions, the fluctuating resistance pinpoints a range in which the material is sufficiently molten that additional effects may be considered. Indentations were easily formed for any temperature exceeding maximum piezo retraction [Figure 9]. As in the case of HDPE, the source voltage limit predominately determines the indentation depth, though the applied contact force was varied between the same three set point values per temperature to assess the influence of increased pressure compared to that on a harder surface.

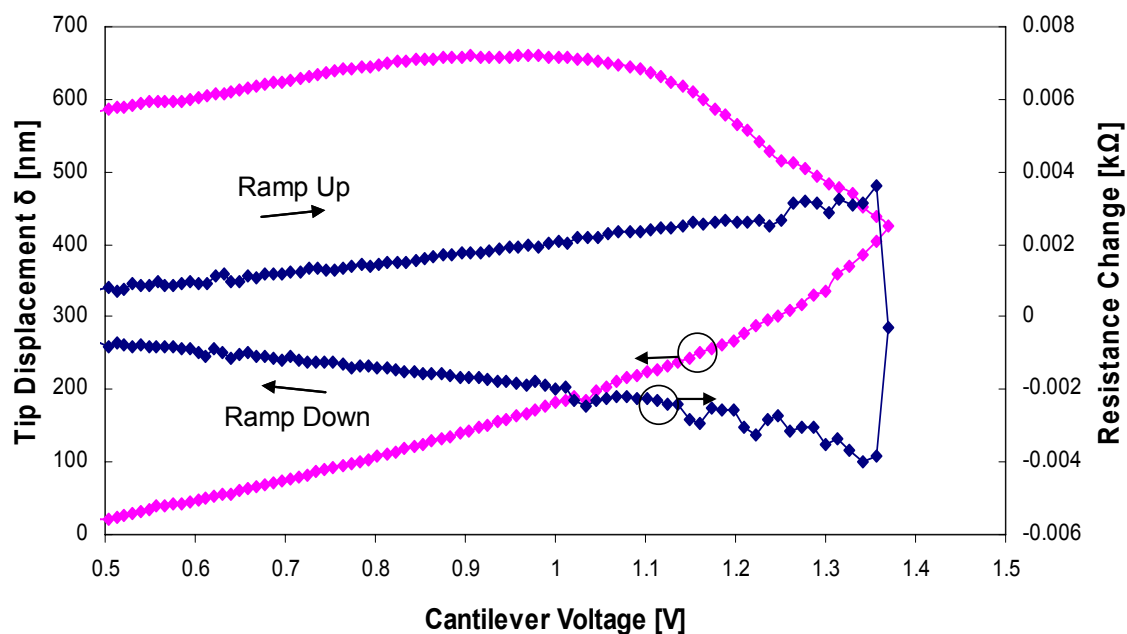


Figure 8. Tip displacement and resistance change for aspirin at 103 nN applied contact force. The onset of softening is given by a gradual downward displacement of the tip. Fluctuations in the resistance change are observed with continued rise in temperature.

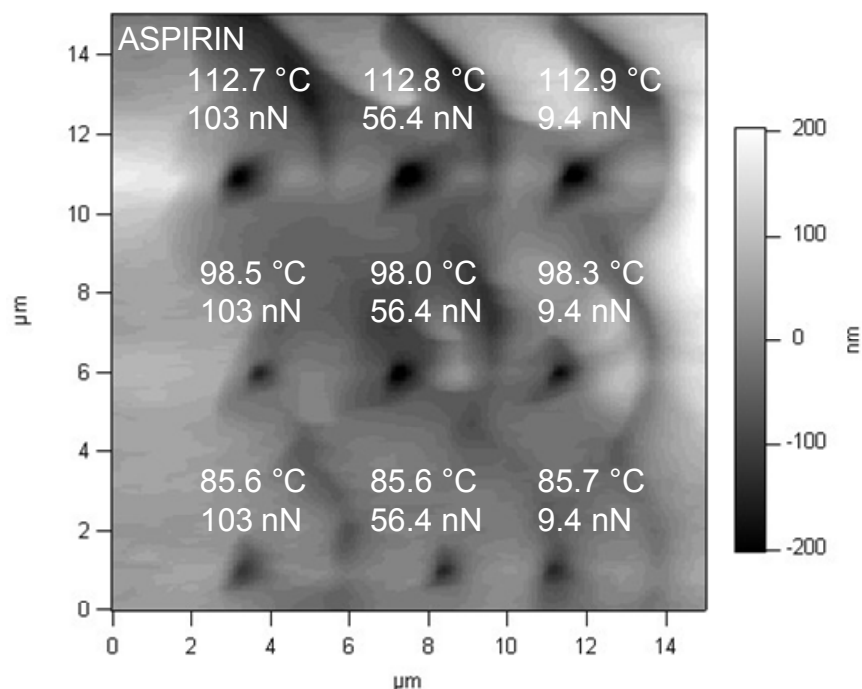


Figure 9. Indents formed by an in-contact temperature ramp on aspirin. Both temperature and contact force were varied; heating and cooling rates were held constant.

2.7 Results and Discussion

Temperatures corresponding to the maximum tip displacement and resistance change on the brink of softening were identified, and average values are provided in summary Figures 10 and 11. For HDPE, the resistance-based transition consistently preceded physical displacement of the tip by roughly three degrees, revealing that the probe senses the thermal event much sooner than the feedback is able to respond. However, the two phenomena are coupled and it is not evident that one should precede the other. For aspirin, the monitored height information was used to identify the transition since there was no corresponding resistance drop. The signals are plotted against the estimated indentation depth.

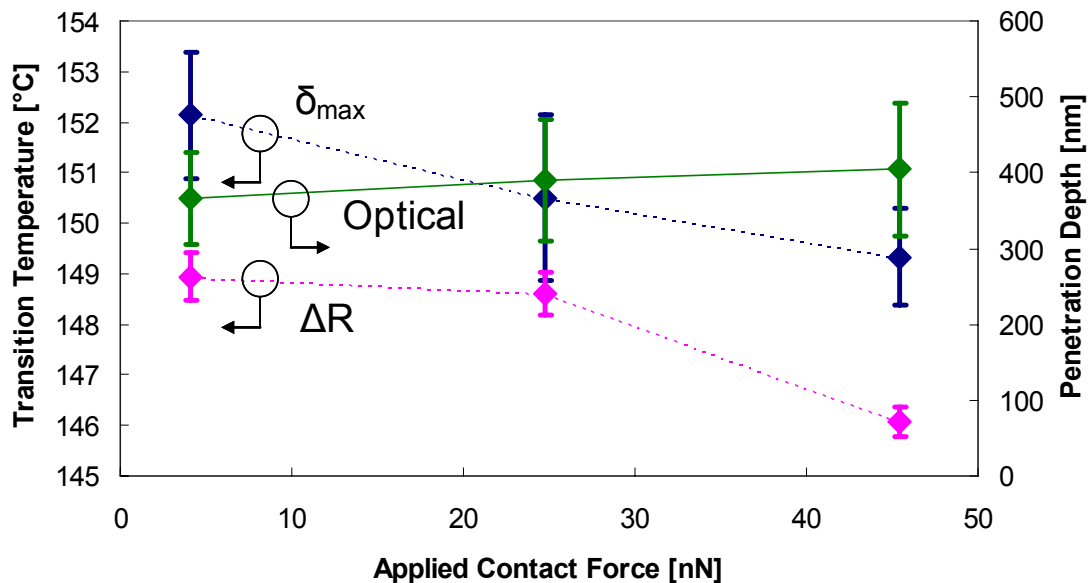


Figure 10. Average temperature transitions and indentation depths for HDPE as a function of contact force. The temperature corresponding to maximum tip displacement and resistance at the onset of softening were identified. Penetration depth was determined by cross-sectional analysis of the processed AFM image.

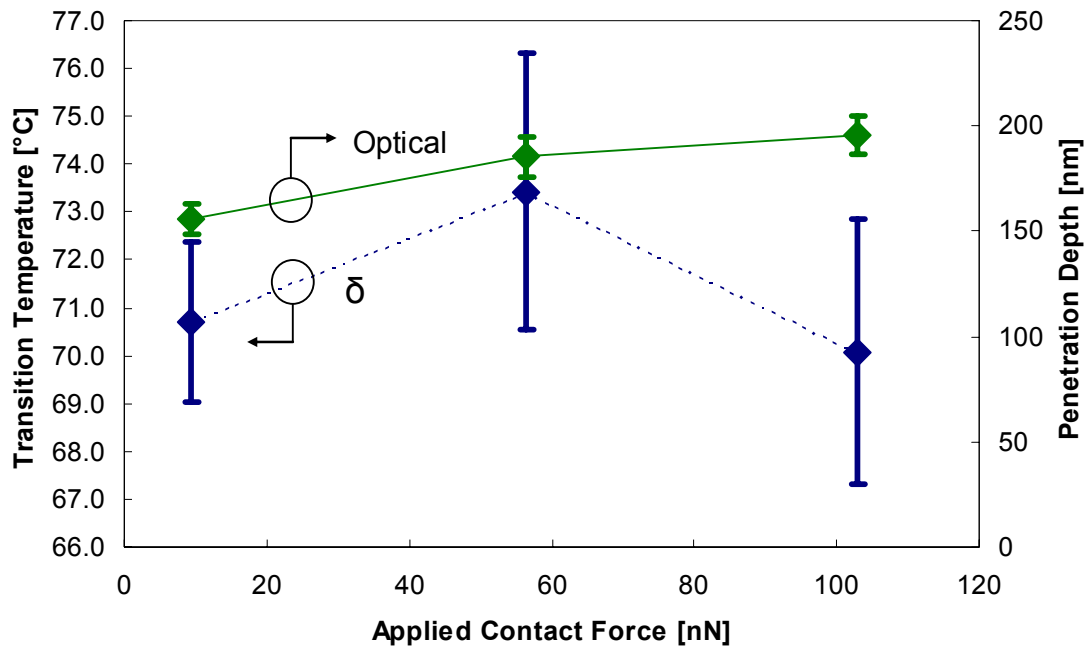


Figure 11. Observed temperature transitions and indentation depths for aspirin. The temperature at maximum tip displacement indicates the onset of softening. A corresponding drop in resistance was not observed.

For HDPE, the calibrated temperature range of the noted transitions was 150-160 °C, which exceeds the expected melting point by at least 15 °C. In contrast, the melting point for aspirin based on tip displacement was at least 65 °C less than the bulk value. The softening point of both substrates demonstrates dependence on the applied contact force. In particular, HDPE provides several opportunities to analyze the force trend. Figure 12 compares the temperature at the onset of piezo extension and subsequent local maximum and minimum temperatures. The average discrepancy between highest (45.4 nN) and lowest (4.13 nN) set point forces was most significant at the onset of downward displacement δ_{\max} , where the transition differed by 2.81 °C. The observed delay was abated with continued submersion of the tip; ensuing T_{\max} and T_{\min} transitions foresaw a maximum difference of 1.38 °C and 1.33 °C, respectively. This is also made evident by

the fact that the rates at which the tip penetrate approach $10 \text{ nm}/^\circ\text{C}$ after the initial temperature upset ceases, regardless of set point force. A maximum $3 \text{ }^\circ\text{C}$ difference based on the δ_{max} transition was also observed for aspirin, though on average the intermediate (56.4 nN) force resulted in the most delayed transition.

The resistance change corresponding to each event can also provide indirect measure of instantaneous heat loss from the tip. For HDPE, the probe senses nearly equal dissipation at all applied forces at the maximum upward displacement and local temperature minimum [Figure 13]. However, at the local temperature maximum, the probe experiences a more significant drop in resistance when it is weakly engaged on the surface. In Figure 13, the changes in resistance are plotted against the source voltages to perceive ‘when’ each event occurs, as this variable is independent of the small resistance fluctuations that affect the temperature trend. For aspirin, the resistance change corresponding to the δ_{max} transition was also similar for each of the applied forces (at approximately $0.002 \text{ k}\Omega$).

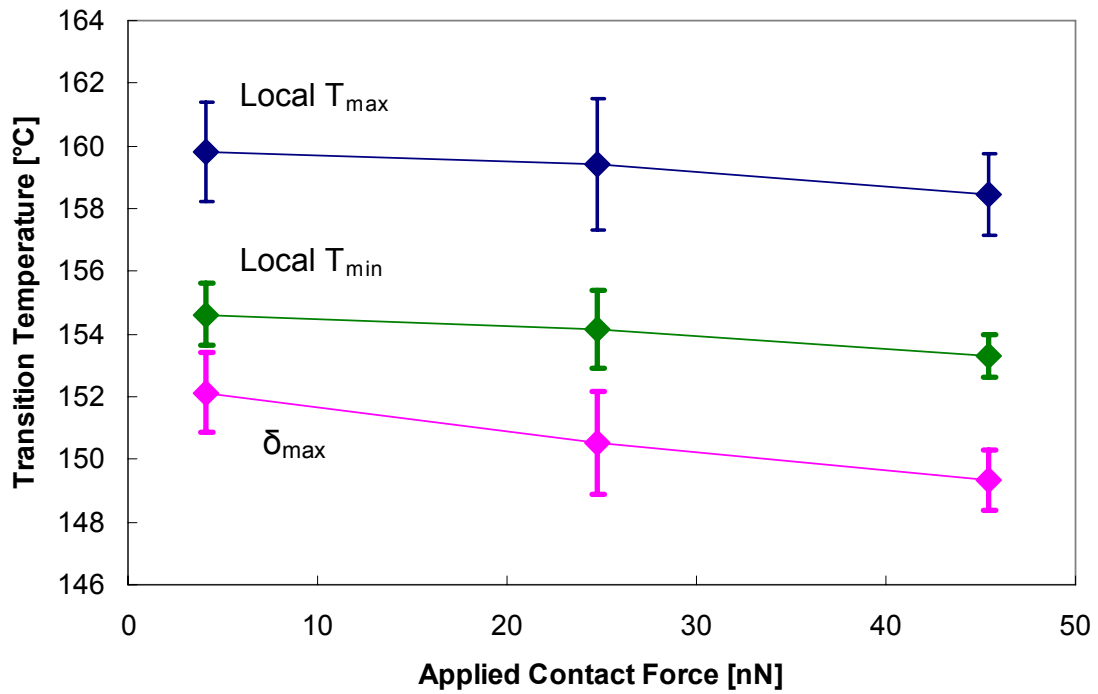


Figure 12. HDPE transitions as a function of contact force. Average temperatures were identified at the onset of downward tip displacement, as well as local maximum and minimum temperature (and resistance) changes for each of the set point forces.

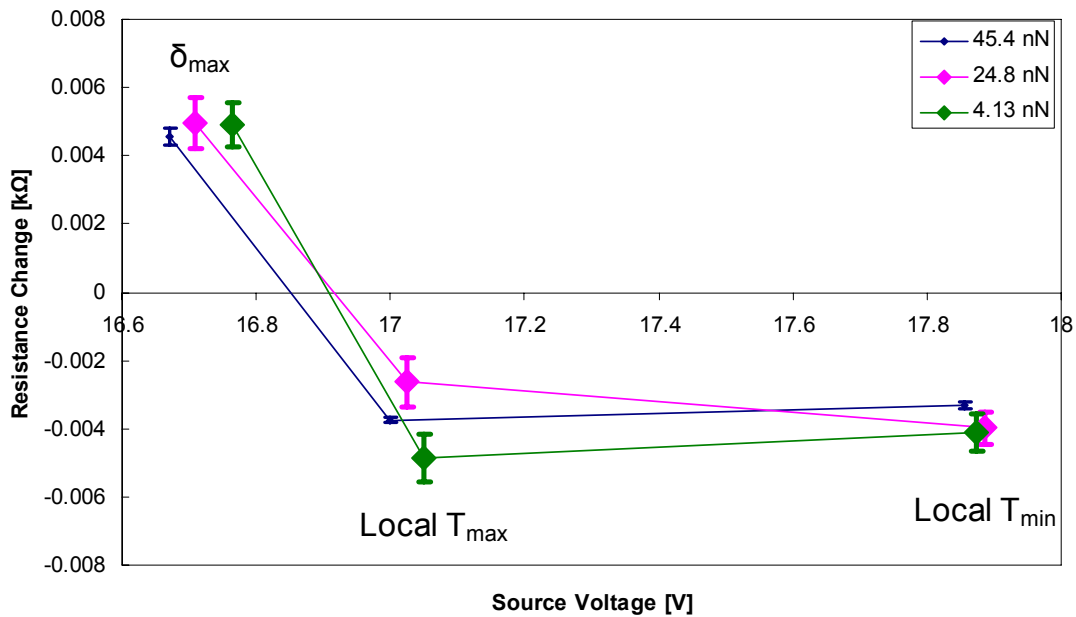


Figure 13. Resistance change at each of the observed HDPE transitions. The values deviate most at the local temperature maximum, which may coincide with initial penetration of the tip into the substrate.

Previous LTMA studies have also reported deviations in the phase transitions of selected polymers and pharmaceuticals [9, 10]. A possible explanation for the discrepancy could be the thermal contact resistance, which is on the order of 10^7 K/W, and is in turn related to the small target volumes and high pressure applied at the tip. Though the data suggests that varying the force affects both material softening points, it is apparent that surface rigidity predominately determines which transitions will be manifest for analysis. For instance, the ‘true’ melting point for HDPE might be regarded as the momentary temperature standstill as opposed to the initial downward tip displacement as portrayed in Figure 5. Since aspirin readily deforms under tip pressure, more intimate contact between tip and surface is achieved to initiate sinking. The melting point of aspirin could therefore be obscured by an enhanced softening rate or the close contact which facilitates steady heat dissipation to the substrate. This method therefore provides an accurate temperature range in which the local phase transformation occurs, but it proves difficult to pinpoint melting by in-contact heating unless the material can somewhat withstand probe pressure as it softens.

For HDPE, mitigating the force consistently delayed the observed transitions, as more power was required to overcome the greater thermal impedance and achieve the same degree of substrate softening. The initially applied force also has less significance as contact area increases and the subsurface material exerts more influence on the sinking tip. However, the resistance trend suggests that there might be a tradeoff between increasing the force such that the displacement rate is largely determined by tip pressure, and decreasing the force so that the tip temperature is slightly elevated at the moment it

comes into closer contact with the subsurface material. The latter case could explain why at the weakest force the tip loses heat most rapidly to the substrate as it penetrates, despite having the most delayed transition. The discrepancy becomes less with continued submersion of the tip as all three forces achieve roughly equal heat loss by the time thermal equilibrium is restored and the temperature continues to rise. A similar argument could be applied to results for aspirin. The tip at an intermediate force of 56.4 nN was perhaps displaced more slowly than when contacting the surface at increased mechanical pressure (103 nN). However, the tip on average moved into closer contact later than when a weaker (9.4 nN) force was applied since the contact resistance (and temperature) was comparatively less.

Meanwhile, the absence of discrete temperature transitions and onset of resistance fluctuations in aspirin could be explained by a quantified ‘pull-in’ effect. The heated probe has been observed to overly deflect in response to adhesive pull from partially molten subsurface material. Force-distance studies have demonstrated that aspirin deviates from other tested analytes in that it shows increased adhesion up to 40 °C below its expected melting point [9]. The adhesive force was also noted to decrease with reduced viscosity. In this study, observed fluctuations arose at temperatures exceeding the initial penetration, suggesting that material viscosity may have been reduced to a point that it intermittently lost adhesive pull on the tip. A changing surface contact area would account for the sudden oscillating heat loss. This effect was gradually diminished as the temperature was stepped down and material viscosity increased.

The measured tip displacement as the temperature is ramped down indicates that both aspirin and HDPE continued to deform under pressure. We would expect to see a

plateau in this signal as it comes into thermal equilibrium and the probe ceases to deflect. However, the adhesive hold on the tip as a consequence of material solidification may explain the continued bending that instructs the piezo to further extend the tip. Prolonged contact with the subsurface material may therefore limit the accuracy of the LVDT sensor measurement on the ramp down. In general, the indentation depth estimated by offline image processing differed from the recorded tip displacement by at least 50 nm. However, these values are estimates measured relative to the surrounding unperturbed ground.

The probe's temperature sensing capabilities may therefore provide more reliable evidence of the phase transition. The temperature of the probe at each event should approach, if not exactly match, the temperature of the contacting material, and any change in the contact surface area is reflected in the measured resistance. Since the measured transitional ranges deviate by more than the 5 °C Raman calibration uncertainty, this may reflect an observable difference between bulk and localized thermal analysis attributable to the contact resistance between tip and surface [10].

The sensitivity of this method is also determined by the spatial resolution of the tip relative to the constituent phases. For example, the transitions characteristic of HDPE may reflect the average response of crystalline and amorphous domains over the tip-surface contact area. If the contact area were comparable to the size of the amorphous regions, local thermal analysis would often result in the absence of an observable transition near the expected melting point. Knowledge of the percent crystallinity and average crystallite size could therefore be used in conjunction with phase contrast imaging to resolve components and interpret the associated local thermal responses.

2.8 Thermally Induced Bending

Cantilever deflection is primarily attributed to submersion of the tip as a direct consequence of material softening, and less significantly with thermally induced bending. However, accurate determination of a material-specific melting temperature warrants characterization of the probe's thermal response. Comparative studies of the contact force were conducted on a glass coverslip, which is expected to deform less than the tested substrates, to ensure that measured tip displacement is indicative of heated deflection. Suggested causes for such bending include disparate expansion coefficients due to the doping profile, and absorption of atmospheric water [22, 23]. While the direction of bending is sometimes difficult to assess during AFM measurements, the deflection signal was observed to consistently increase with cantilever voltage with and without feedback control. In particular, the free range deflection far from the substrate for consecutive heating cycles was compared to that on the glass surface to assess the restriction imposed by feedback as a function of the set point force.

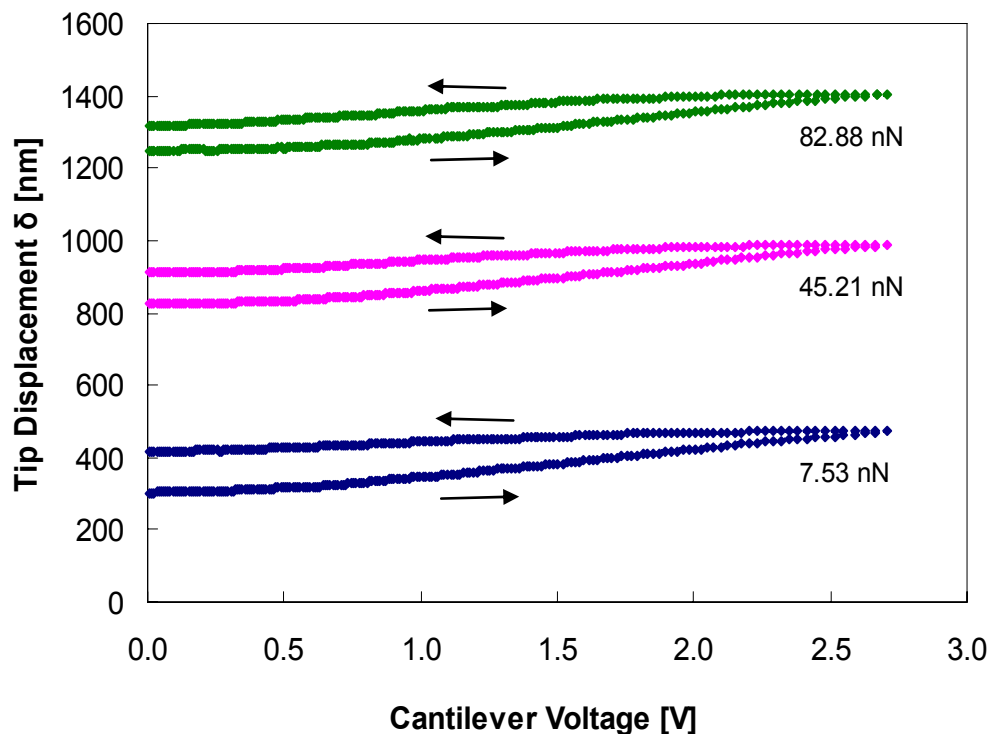


Figure 14. Extracted LVDT signal on glass for various contact forces. The cantilever was heated and cooled with the tip engaged on the surface. The probe is displaced by a given distance to account for heat-induced deflection and maintain set point force.

Ideally, we would track zero displacement for a probe engaged on glass during a temperature ramp. However, several factors contribute to the observed upward displacement [Figure 14]. The piezo is subject to drift, but the effects are random and insignificant over the time scale elapsed per characterization. Secondly, the glass may not be entirely rigid underneath tip pressure. Finally, it was demonstrated by turning the feedback off with the probe far from interaction with the surface that unhindered deflection increases with temperature. With the tip engaged, such motion is significantly restricted. Applying more pressure to the tip as it heats enhances deflection and the distance the piezo must retract the tip to compensate. By fitting each upward displacement with a second order polynomial, it was determined that the weakest contact force resulted in overall less retraction. Therefore, it is expected that initially, the net

downward displacement as a consequence of substrate softening will increase as less pressure is applied at the tip.

Figure 15 demonstrates that unrestricted thermally induced bending is most significant on the initial temperature ramp and stabilizes with consecutive runs. To minimize this effect, the probe was ramped several times prior to each experiment. An apparent delay between the maximum voltage sourced and maximum deflection attained suggests that bending does not cease until some point on the ramp down. Similarly, the probe does not fully relax until some time after the voltage is stepped back to zero. Therefore, heated deflection likely contributes to the net displacement signal, but is expected to have minimal impact for a given set point force due to the consistent bending of the probe on the temperature ramp.

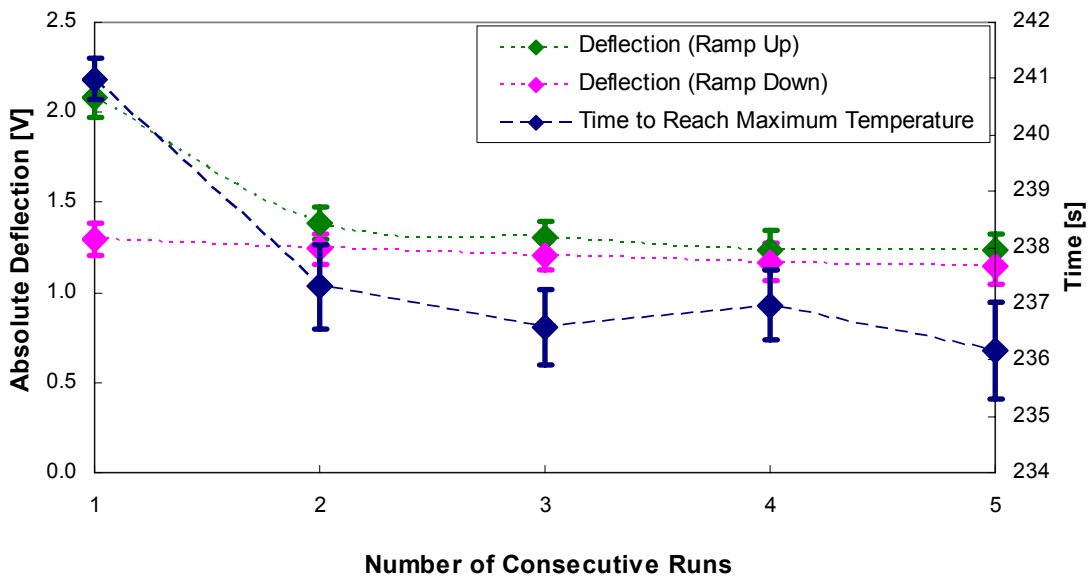


Figure 15. Heat-induced bending. The maximum probe deflection is compared separately for heating and cooling during five consecutive temperature ramps. Both deflection on the ramp up and the time required to reach maximum temperature decrease and stabilize after the initial run.

CHAPTER 3

FEASIBILITY EXPERIMENT WITH A HEATED KELVIN PROBE

In scanning Kelvin probe microscopy (SKPM), a conductive tip is scanned at fixed distance above a biased sample under AC driving voltage. The target contact potential, which measures the electrostatic field arising between the two electrodes, is the DC voltage required to null the cantilever oscillations. The first pass captures the topography and the second detects variations in the potential offset between tip and sample. The objective of this chapter is to ascertain whether the heated silicon probe functions as a capable electrode for SKPM applications. This was achieved by performing heated force-distance experiments on a biased gold film with the tip operating at various potentials.

3.1 Experimental Method

The cantilever tested in this study is characterized by a triangular free end (173 μm sides, 87 μm base) that was lightly doped to $1 \times 10^{17} \text{ cm}^{-3}$ during fabrication such that it achieves a temperature of approximately 610 $^{\circ}\text{C}$ at thermal runaway. For operations below this temperature, heater resistance is akin to temperature and determined largely by the impurity concentration [19]. The cantilever legs span 670 μm in length and are doped to $1 \times 10^{20} \text{ cm}^{-3}$ such that the gradient along the legs is small compared to that within the heater region and extending along the tip. Raman calibration by the shifting Stokes peak method was used to ascertain the probe temperature in close contact with the unbiased surface. In particular, a voltage ramp in contact with gold at approximately 37.1 nN applied force yielded 52.1 $^{\circ}\text{C}$, 95.7 $^{\circ}\text{C}$, and 157.1 $^{\circ}\text{C}$ for the target values. The

temperature sensed by the probe increased to 75.4 °C, 126.9 °C, and 198.9 °C by withdrawing the tip roughly 6 μm from the surface.

Prior to each trial, the probe was ramped to threshold voltage in series with a protective 9.8 kΩ resistor to establish electrical consistency. Reference force-distance measurements were then taken at room temperature with zero potential across the tip. A circuit pertaining to each of the three schemes was assembled. The second unheated standard was accomplished by joining the legs such that the tip potential equaled the voltage supply as indicated in Figure 16. The heated unbiased trial comprised sourcing voltages of equal and opposite magnitude to each leg such that potential drop was effectively nulled [Figure 17]. Finally, the probe was both heated and biased by sourcing current to one leg and grounding the other; in this case, the tip potential is presumed to be half of the total difference [Figure 18]. Voltage supplied to probe and sample were measured; for the heated trials, current and power dissipated by the cantilever were also recorded.

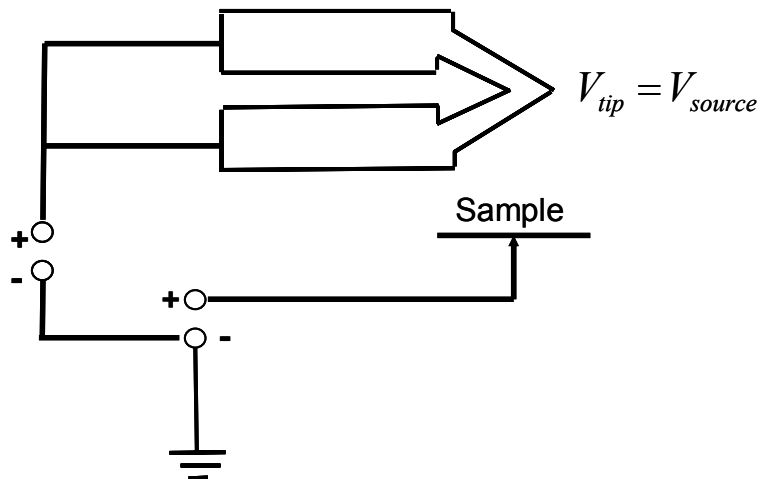


Figure 16. Circuit diagram for the case in which the tip is both unheated and biased (and potential on tip nearly equals source voltage).

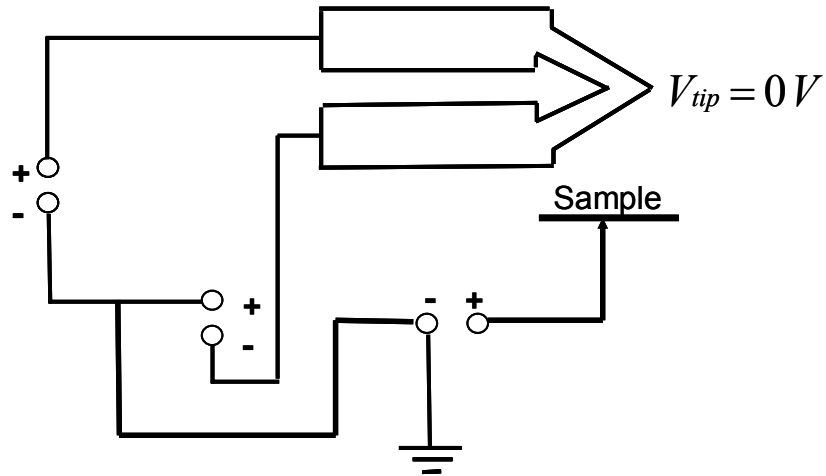


Figure 17. Circuit diagram for the case in which the tip is heated but unbiased.

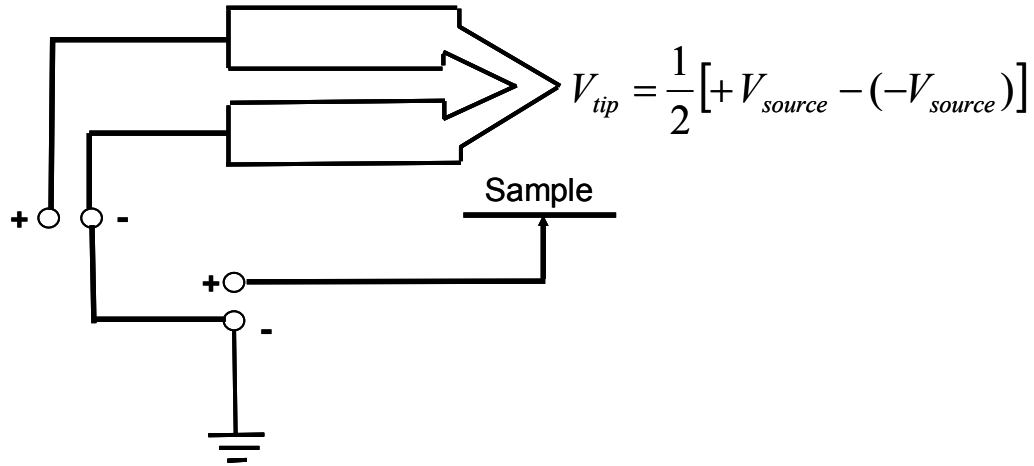


Figure 18. Circuit diagram for the case in which tip is both heated and biased (and the potential on tip is approximately half of the total potential across the legs).

Extension of the z piezo stack lowers the cantilever into attractive range of the substrate, after which it is manually engaged at a contact force of approximately 40 nN and extends farther with the sample into the mid-range of the z piezo input voltage. The tip is then withdrawn from the surface and the circuit powered. For each of the above trials, the probe was allowed to reach steady state before calibration within the MFP 3D Igor Pro software. First, the virtual deflection was corrected with a free range force-distance measurement to account for the mechanical coupling between piezo stack and

deflection output that is responsible for any non-physical interaction between tip and sample during the approach (essentially reducing the noise level from 40 μm to 1 nm). The probe was then engaged on the 100 nm gold film and a preliminary curve taken with zero bias to obtain the deflection inverse optical lever sensitivity (invOLS). The spring constant was calibrated directly from this value via the thermal noise method, in which the resonant frequency was identified from a thermal power spectrum taken several millimeters from the surface. The spring constant was determined to be roughly 0.15 N/m but softened to 0.10 N/m at the highest temperatures.

An illustration of the force-distance measurement is provided in Figure 19. The attractive force between tip and sample increases on approach until the tip abruptly snaps into contact and deflects under continued piezo extension. On retraction from the surface, the release is displaced farther from the surface than the initial contact point. The sample bias reduces the observed deflection relative to the background and introduces curvature at the snap-in point proportional to its magnitude [Figure 20]. Due to the selected trigger channel, the raw data is output as deflection versus LVDT travel in units of distance, but captures the information necessary for conversion to a force-distance curve [24].

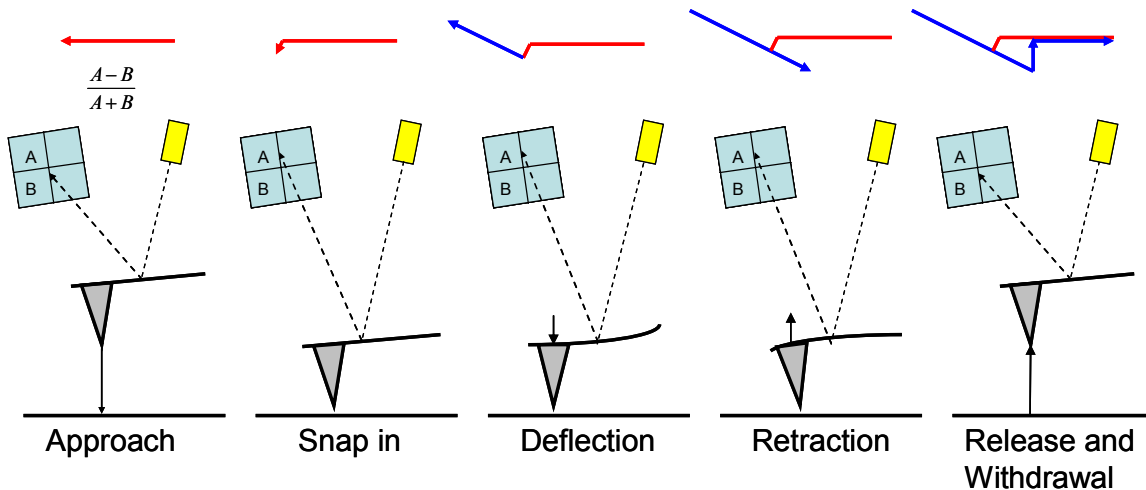


Figure 19. Force-distance measurement. The piezo lowers the tip into the attractive range of the surface. The tip abruptly snaps into contact and feedback adjusts the height so that the free position vertical deflection matches set point value. The tip continues to deflect in contact until the trigger point is reached, after which it is retracted. The tip is released from the surface at a distance greater than initial snap-in.

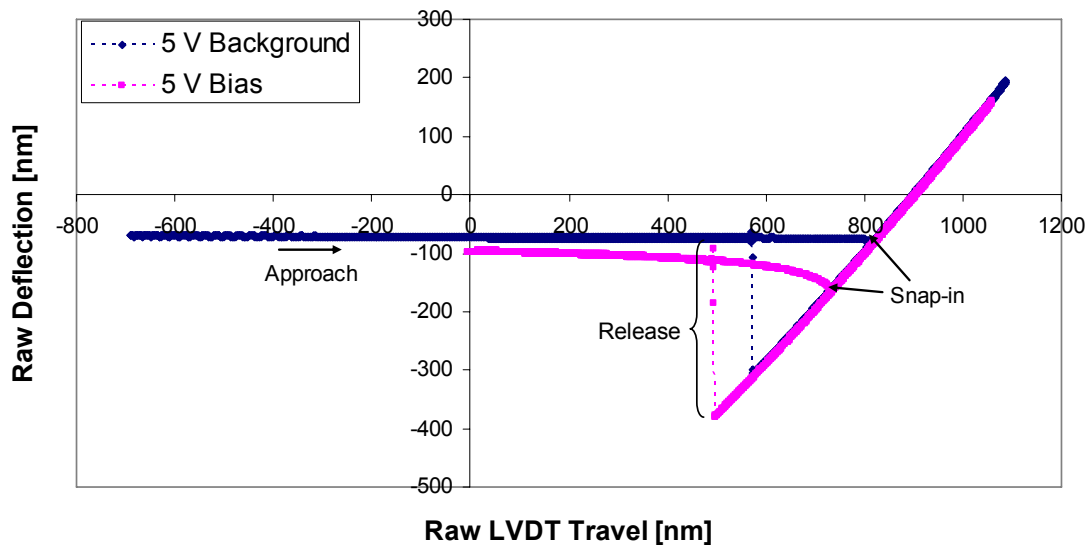


Figure 20. Example raw deflection – LVDT output for a sample bias of + 5 V and for a probe at approximately 70 °C with + 0.5 V bias on the tip.

The sample was randomly biased from + 9 V to -9 V with the tip withdrawn from the surface. Each bias was preceded by a 0 V background measurement. In contrast, the temperature and potentials applied to the tip were not manually adjusted during the trials. To ensure that the piezo swept through constant distance for each measurement, a trigger

point of 1 V designating the turn-around point was set relative to the initial deflection. This compensates for any drift of the laser spot within the optical path that would otherwise reduce or extend the traveled distance proportional to an absolute 1 V trigger point. For all trials, a constant piezo approach velocity of 2 $\mu\text{m/s}$ based on force distance of 1 μm and scan rate 1 Hz was maintained such that heat dissipation to the gold surface was a function of separation distance and not the associated time constant.

3.2 Analytical Approach

3.2.1 Contact Potential Measurement

The primary goal is to extract the contact potential V_C – a parameter which encompasses material properties of both tip and sample and quantifies nonequilibrium charge distributions induced by the field emanating between them. To do so, we can analyze the force governing their interaction as a function of separation distance. The force measurement captures not only the net attraction due to their disparate potentials, but also the electrostatic field induced by a preexisting temperature gradient [Figure 21]. We can therefore assess the influence of temperature on the contact potential which arises as a result of the Seebeck effect [25].

The tip was biased at six voltages (three magnitudes above and below ground) and three temperatures spanning 70 to 200 $^{\circ}\text{C}$. An unbiased tip was identically tested with and without the influence of heat in order to establish benchmarks to which the above schemes could be compared. In this way, the response of the tip due to thermal effects could be isolated from those dependent on the driving voltage.

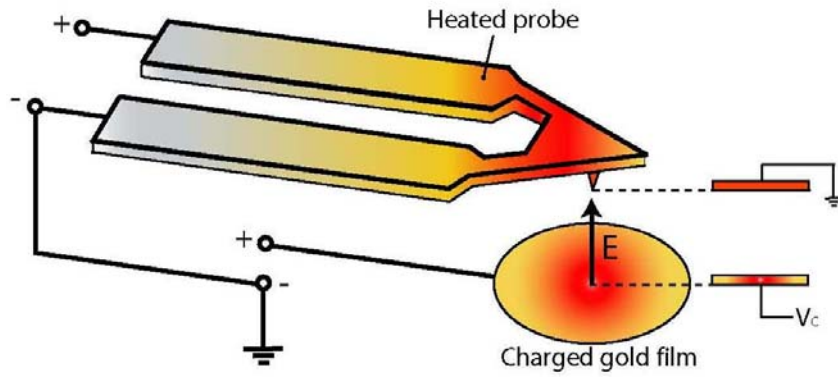


Figure 21. Heated Kelvin probe. The tip and sample may be regarded as two capacitive electrodes. The direction of the electrostatic field emerging between them is determined by the difference between sample bias and contact potential. The contact potential is a measure of the voltage that could be applied to the sample to null the field. By definition, V_C accounts for the tip bias, silicon surface potential, silicon-gold work function difference, and the thermal voltage arising as a result of the Seebeck effect.

During a force-distance measurement, the tip and sample may be regarded as two capacitive electrodes with a work function difference that contributes to the measured contact potential describing the nature of their interaction. As the silicon tip is moved in proximity to a charged conducting surface, the ensuing electric field induces carrier mobility and redistributes charge between surface and bulk silicon, thus affecting the surface potential. The contact potential is in part defined by the surface potential as follows:

$$V_C = V_s + (W_{Au} - W_{Si})/e \quad (2.1)$$

where W_{Au} and W_{Si} are the work functions of gold and silicon, respectively, and V_s is the surface potential of silicon. The lack of a contributing gold surface potential is due to its conductivity; any localized bias originating from contact with the tip will be immediately and uniformly dissipated throughout the material. Rather, the applied sample bias serves to enhance or mitigate the strength of the field and governs transitions between the silicon surface charge states.

The thermoelectric effect is given by:

$$\Delta V = \int_{T_o}^T S(T) dT \quad (2.2)$$

where the Seebeck coefficient S is sensitive to the temperature-dependent doping concentration as well as the temperature [26]. For an n-doped semiconductor, the Seebeck coefficient is by convention negative, since electrons migrate with heat and the unheated destination (the sample) is then negative with respect to the source. In contrast, the Seebeck coefficient for gold is a positive quantity with a bulk literature value two orders of magnitude less than that of silicon [Table 1]. With regard to both the temperature gradient and applied bias across the cantilever legs, we may express the contact potential as follows:

$$V_C = V_S + (W_{Au} - W_{Si})/e + V_{tip} + \int_{T_o}^T S(T) dT \quad (2.3)$$

The work function and surface potential of silicon also depend on temperature but are not assumed to vary significantly as a result of the gradient unless the tip is characterized by a high density of surface states. Therefore, the contact potential difference between heated and unheated cases is thought to depend on the driving voltage and thermoelectric power.

3.2.2 Seebeck Coefficient

In general, the Seebeck coefficient may be calculated [27]:

$$S = -\frac{k_B}{e} \int \left(\frac{E - E_f}{k_B T} \right) \frac{\sigma(E)}{\sigma} dE \quad (2.4)$$

in which the energy E is referenced to the Fermi level E_f and depends on the material-specific conductivity σ , Boltzmann constant k_B (1.38×10^{-23} J/K = 8.62×10^{-5} eV), and elemental charge e (-1.602×10^{-19} C). For the extrinsic n-type semiconductor, the coefficient may be rewritten in terms of conduction band edge E_C , and a weighted average A_C that accounts for carriers distributed beyond E_C :

$$S = -\frac{k_B}{e} \left(\frac{E_C - E_f}{k_B T} + A_C \right) \quad (2.5)$$

The above expression was evaluated for the target temperatures with $A_C = 2$, given that the difference

$$E_C - E_f = -k_B T \ln \left(\frac{n_o}{N_C} \right) \quad (2.6)$$

also depends on n_o , the doping concentration at room temperature, and N_C , the effective density of state at the conductive band edge. In turn, the density of state is given by:

$$N_C = 2 \left(\frac{2\pi m_n^* k_B T}{h^2} \right)^{3/2} \quad (2.7)$$

in which Plank's constant $h = 6.634 \times 10^{-34}$ J·s, and the effective mass of the electron m_n^* is related to the universal mass $m_o = 9.11 \times 10^{-31}$ by a factor of 1.08 for crystalline silicon [28]. Table 1 provides calculated coefficients for selected doping levels. Annealing during fabrication diffuses added impurities into the bulk, though the spatial profile may

extend from a surface concentration of $1 \times 10^{17} \text{ cm}^{-3}$ or $1 \times 10^{20} \text{ cm}^{-3}$ to the base silicon value of $1 \times 10^{14} \text{ cm}^{-3}$.

Table 1. Seebeck Coefficients for Doped Silicon [V/K]

	300 K	340 K	400 K	470 K
Silicon, $n_o = 1 \times 10^{14} \text{ cm}^{-3}$	-12.5×10^{-4}	-12.7×10^{-4}	-12.9×10^{-4}	-13.1×10^{-4}
Silicon, $n_o = 1 \times 10^{17} \text{ cm}^{-3}$	-6.59×10^{-4}	-6.75×10^{-4}	-6.96×10^{-4}	-7.16×10^{-4}
Silicon, $n_o = 1 \times 10^{20} \text{ cm}^{-3}$	-0.630×10^{-4}	-0.792×10^{-4}	-1.00×10^{-4}	-1.21×10^{-4}

Trapezoidal integration of each Seebeck-temperature curve yields the predicted thermal voltages, assuming a maximum temperature gradient (with respect to 300 K):

Table 2. Thermal Voltages [V]

	340 K	400 K	470 K
Silicon, $n_o = 1 \times 10^{14} \text{ cm}^{-3}$	-0.0505	-0.127	-0.219
Silicon, $n_o = 1 \times 10^{17} \text{ cm}^{-3}$	-0.0267	-0.0678	-0.117
Silicon, $n_o = 1 \times 10^{20} \text{ cm}^{-3}$	-0.00285	-0.00825	-0.0160

Since heat generation is primarily confined to the lightly doped ($1 \times 10^{17} \text{ cm}^{-3}$) free end, the gradient from bridge to tip is assumed most significant [18]. The heavily doped cantilever legs ($1 \times 10^{20} \text{ cm}^{-3}$) are expected to contribute less to the thermal voltage. Due to localized heating of the sample, the Seebeck coefficient of gold will also contribute to the integral term as a function of temperature. Gold has a coefficient of $2\text{-}2.5 \times 10^{-6} \text{ V/K}$ at room temperature [29], which is expected to vary less with heat than that of the semiconducting tip.

3.2.3 Electrostatic Force

The electrostatic force, which varies with the square of the tip-sample distance, may also be expressed in terms of the contact potential:

$$F = F_{bg} + f(d)(V_b - V_c)^2 \quad (2.8)$$

where $f(d)$ is a capacitive coupling dependent on the separation distance d as well as the tip geometry, and V_b is the sample bias. F_{bg} represents any nonvoltage-dependent background force, including long range attractive van der Waals forces, which are accounted for by subtracting from each force-distance curve an unbiased sample measurement taken in the immediate vicinity of each applied sample bias. By comparing the above relation with a parabolic fit of the force-sample bias plot,

$$F = p_1 V_b^2 + p_2 V_b, \quad \text{we obtain: } V_c = -\frac{1}{2} \frac{p_2}{p_1}. \quad (2.9)$$

The contact potential corresponds to the x-offset of the unbiased case from zero force. Physically, it represents the voltage required to null the electrostatic field that arises as a result of the work function difference and other contributing factors. This relation holds for all biases and temperatures which may be applied to the probe.

3.2.4 Space Charge Effect

For a semiconducting tip or sample, the measured force and extracted contact potential are sensitive to the effects of space charge [30]. The onset of depletion is not of particular concern for the results presented here as it necessitates a tip at extreme positive potential subject to a negative sample bias. The maximum potential applied to the tip is +1 V, which coincides with a state of accumulation for much of the bias range (-4 to +9

V). The direction of the field is determined by the difference between driving voltages; therefore, positive and weakly negative sample biases will induce a build-up of electrons on the tip surface. Only the extreme negative bias will reverse the field, resulting in formation of a space charge layer extending into the bulk. If the effect persists to further increase the concentration of acceptors within the layer, the tip enters a state of inversion. This scenario is manifest in the force-sample bias plot by skewing the negative bias data such that the offset then deviates from a linear trend. However, this effect is reduced with the tip potential as the onset of depletion shifts toward more negative biases. For example, the minimum -1 V tip bias is predicted to maintain accumulation for all sample biases greater than -6 V. The possible transition between surface states as a consequence of the driving voltage difference is illustrated in Figure 22.

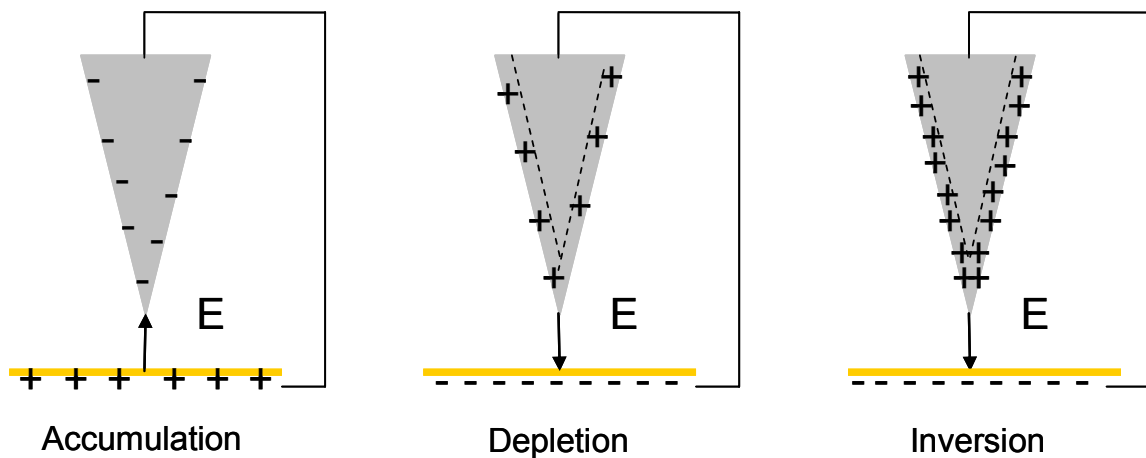


Figure 22. Possible surface charges states on the silicon top. An extreme negative sample bias with the tip at positive potential could result in the onset of depletion and the formation of a space charge layer. Most tip-sample bias combinations correspond to a state of accumulation.

3.3 Results and Discussion

Raw data was processed in the following way: first, the snap-in point was identified and regression was performed on all data points between initial contact and the trigger point.

The measured approach distance and deflection were then normalized by the slope (invOLS) specific to each curve to correct for instrumental drift. The data was interpolated at a distance of 20-150 nm before contact and converted to a force measurement as follows:

$$F = k(H - H_b) \quad (2.10)$$

where k is the precalibrated spring constant and H and H_b are the measured deflections of the bias and background, respectively. The total distance traveled by the tip was determined by adding the LVDT travel to the deflection. Typical force-distance curves are provided in Figure 23.

We may also derive an expression for the normalized force at fixed distance:

$$\Delta F = F(V_b) - F(0) = V_b^2 - 2V_bV_C \quad (2.11)$$

$$\frac{\Delta F^1}{\Delta F^0} = \frac{V_o^2 - 2V_bV_C^1}{V_o^2 - 2V_bV_C^0} = \frac{V_o^2 - 2V_b(V_C^0 + \Delta V_C)}{V_o^2 - 2V_bV_C^0} = 1 - \frac{2\Delta V_C}{V_b - 2V_C}$$

which aids in interpretation of the corresponding normalized plot [Figure 24]. In the above equation, ΔF^1 and ΔF^0 pertain to the heated and unheated cases, respectively. The deviation that occurs at +1 V may be explained in terms of the driving potential: the negative normalized force ($\Delta F < 0$) is an exception and corresponds only to cases in which the tip is at positive bias such that the contact potential is shifted to a positive offset and $0 < V_b < 2 V_C$. For other trials in which negative potential or heat is applied to the tip, a negative shift in contact potential results in a positive normalized force ($\Delta F > 0$) at +1 V, since it corresponds to the scenario $V_b > 2 V_C$ or $V_b < 0$. The increase in magnitude upon approaching zero, particularly for the heated unbiased case, is due to the

fact that the measured forces become comparable to the unheated, unbiased data by which they are normalized.

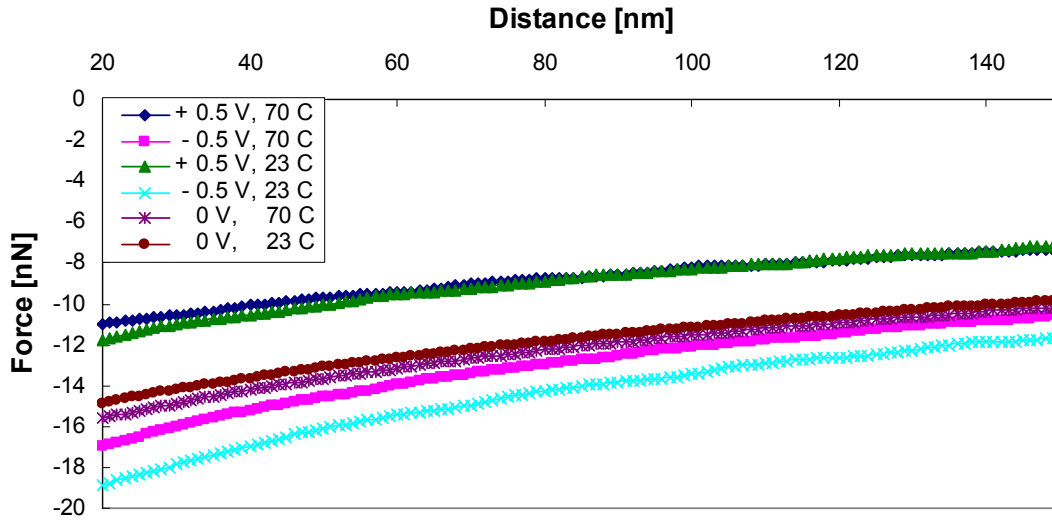


Figure 23. Example force-distance plot in which both tip bias and temperature are varied. The tip experiences increased attractive force on approaching the surface.

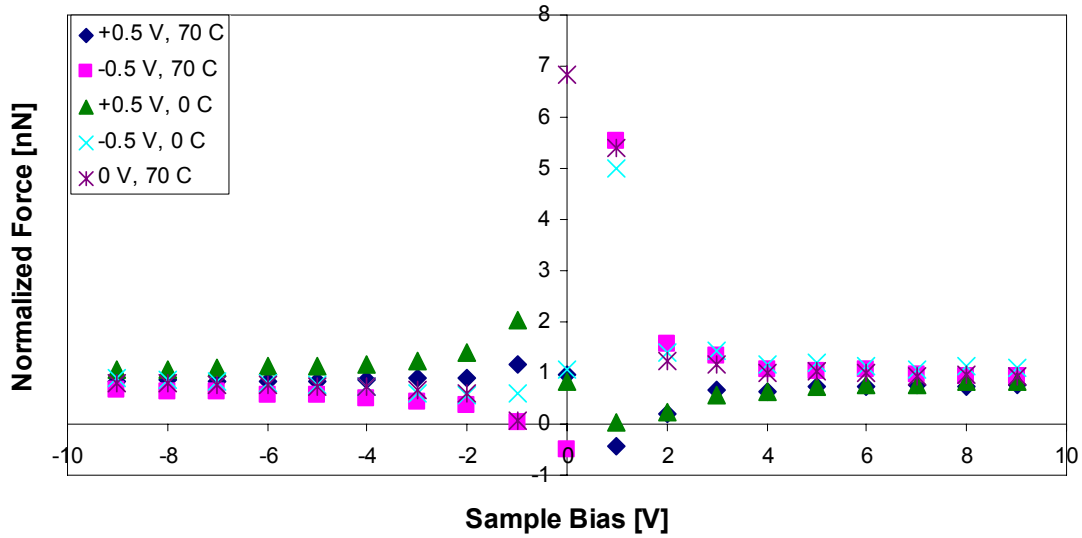


Figure 24. Normalized result 100 nm from contact. All data is normalized with respect to the unheated, unbiased case. The results particularly diverge at + 1 V due to the change in the magnitude of the contact potential relative to the sample bias.

Parabolic regression of the force-sample bias plot with a least squares fit determined the contact potential within a 95% confidence interval. The offset is apparent by comparing an isothermal case in which the tip was biased at ± 1 V and 0 V [Figure 25]. The positive and negative tip potentials are symmetric about the unbiased tip trial, but are not symmetric about the unbiased sample due to the inherent work function difference between the two electrodes. The precalibrated spring constant specific to each trial will translate the parabola in the y-direction, whereas only the presence of space charge affects curvature. As mentioned previously, this is evident by examining the force trend for a given trial at particularly low sample biases.

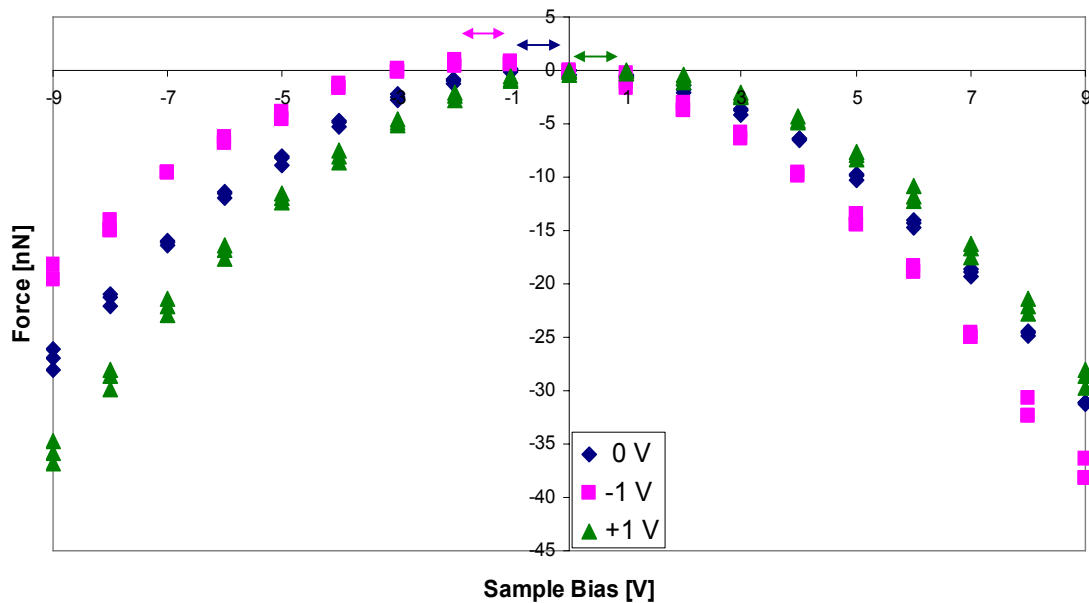


Figure 25. Observed contact potential shift 100 nm from contact for various tip biases and a probe temperature of approximately 200 °C.

The extracted contact potential can then be analyzed as a function of separation distance, with the y-intercept pertaining to the situation in which the work function difference and surface potential balance the applied driving and thermal voltages. The

example provided [Figure 26] demonstrates how the Seebeck effect shifts the potential to greater offsets for a given tip bias. There is little dependence of the contact potential on distance since the data is presented at least 20 nm prior to the snap-in point. For the heated trials, however, a slight increase in the potential shift with distance may be attributed to the fact that the tip temperature is elevated upon retraction from the surface; therefore, the thermally induced voltage exerts greater influence on the electrostatic field.

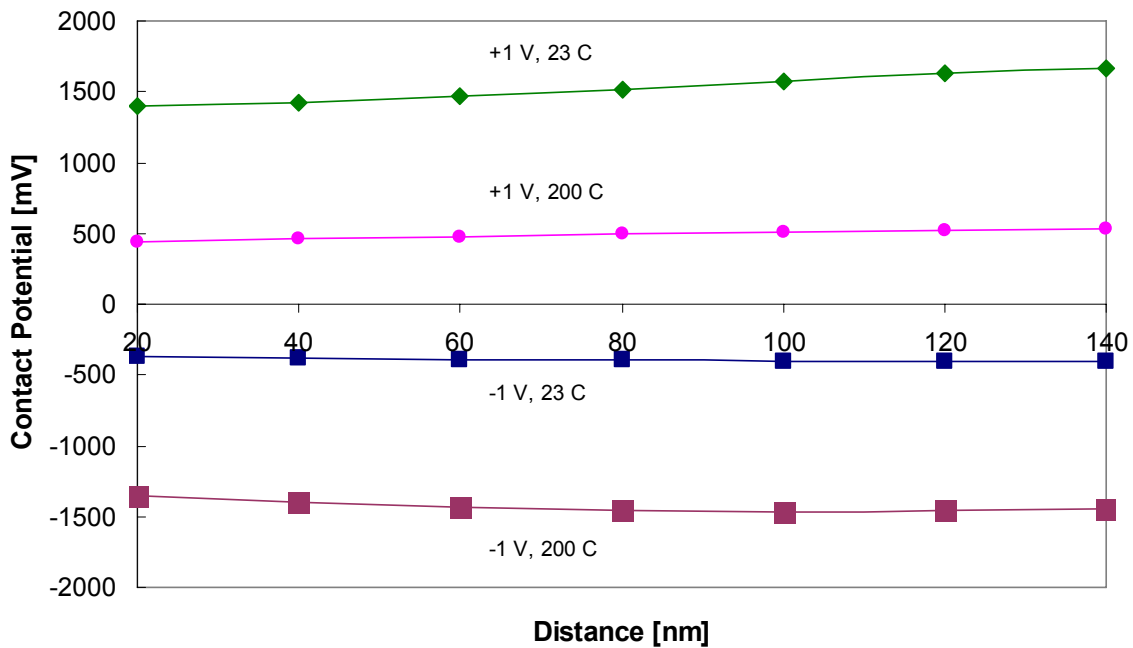


Figure 26. Measured contact potential as a function of distance. Beyond 20 nm from the surface, the contact potential does not vary significantly with distance (though it demonstrates slightly more dependence on distance for the heated case than the unheated).

Based on the thermal voltages calculated in Table 2, the lightly doped case ($1 \times 10^{14} \text{ cm}^{-3}$) at approximately 200 °C yields an estimated value of -219 mV, which is the closest calculated value approaching (and yet significantly less than) a measured contact potential shift of approximately -640 V at the same temperature and 0 V tip bias. The contact potential is defined by the tip bias, work function difference, and surface potential

of silicon. While the first contribution (the tip bias) can be measured, more precise knowledge of the doping profile through the tip and legs is required to predict the silicon-gold work function difference and surface potential of silicon at each temperature. This information is also needed, along with the temperature gradient, to calculate the spatially varying Seebeck coefficient. In addition, the contributing gold work function and thermoelectric power must be accounted for.

The results may be summarized in two plots which portray the effect of temperature on the measured contact potential. In Figure 27, we observe a nearly linear trend that is symmetric about the unbiased tip case specific to each heated trial. Raising the probe temperature shifts the contact potential to greater offsets (given by the parallel lines). However, the offset between two consecutive temperature lines also decreases with applied heat. This is further illustrated in Figure 28, in which the unbiased tip (intercept) data is plotted against the probe temperature.

The uncertainty in Figures 27 and 28 is obtained by dividing the contact potential expression by its differentiated form:

$$\left| \frac{dV_c}{V_c} \right| \leq \left| \frac{dp_1}{p_1} \right| + \left| \frac{dp_2}{p_2} \right| \quad (2.12)$$

Where p_1 and p_2 are the regressed parameters and dp_1 and dp_2 are the corresponding ranges in which they fall to within 95% confidence.

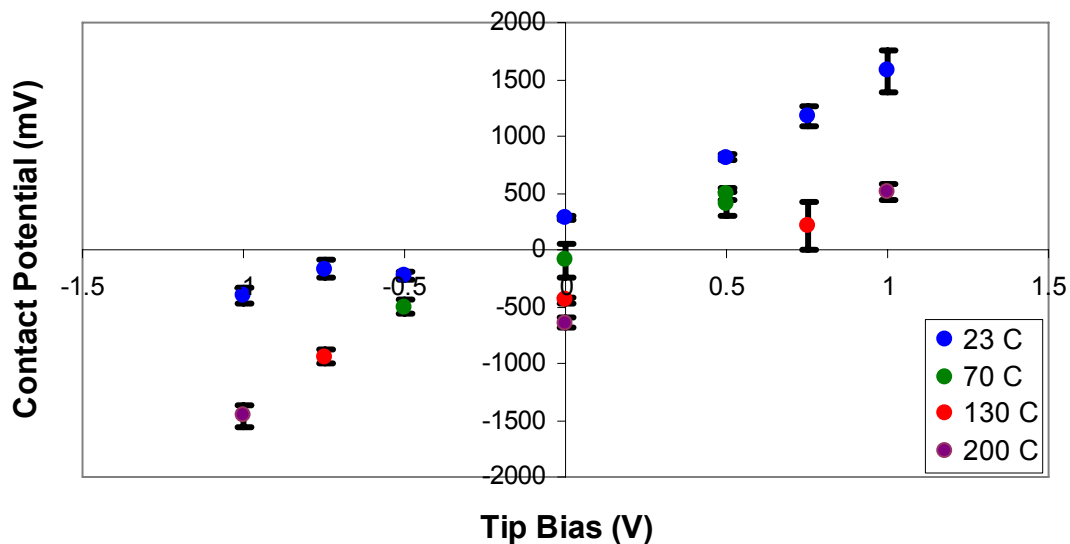


Figure 27. Effect of temperature on measured contact potential 100 nm from contact. The trend is nearly linear and symmetric about each unbiased tip result; the contact potential is shifted to increasingly negative offsets in proportion to the Seebeck effect. The measured contact potential can be either negative or positive depending on the magnitude of the tip bias.

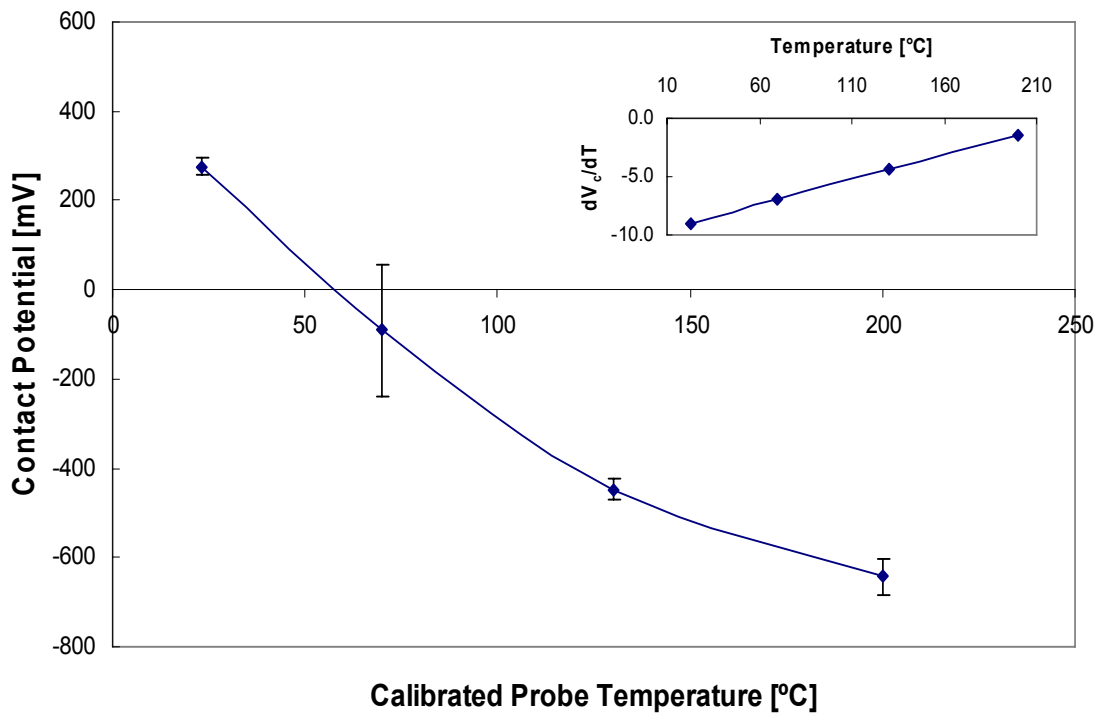


Figure 28. Effect of temperature on unbiased tip. Heat decreases the contact potential such that the direction of the field is from sample to tip (the reference). The contact potential represents the voltage that could be applied to minimize the force between the two electrodes.

In Figure 27, the contact potentials corresponding to + 1 V (the most likely cases to be affected by the onset of depletion) do not deviate from the linear trend. Therefore, it appears that the tip is characterized by a state of accumulation for the range of biases tested here. Assuming a negligible change in the work function difference and the silicon surface potential, the trend in contact potentials is governed by the tip bias and thermal voltage. A negative contact potential describes a field extending from the sample to the tip; however, the sample bias influences the direction of the net electrostatic field.

In Figure 28, the contact potential shifts from a positive offset at room temperature to an increasingly negative offset with added heat, due to the fact that the negative thermal voltage grows in magnitude with the temperature gradient. However, as shown in the inset, the rate of the contact potential shift steadily decreases with increasing temperature. This might be attributed to the spatial dependence of the Seebeck coefficient on the doping profile. Heating the probe may redistribute impurities in the cantilever tip, bridge, and legs such that the coefficient and corresponding voltage are reduced. The contributing gold Seebeck coefficient could also be affected by the temperature change; since the scan rate was held constant, the propagation of heat into the sample and induced electron mobility is determined by the temperature gradient. Thermal bending is not expected to influence the force-distance measurement as the cantilever was allowed to reach steady state before each trial. A surface phase transformation is also unlikely since the probe was operated in a temperature range below the melting point of the gold film.

The results of this experiment therefore demonstrate that the strength of the electrostatic field between tip and sample strongly depends on the probe temperature.

However, the thermal voltage associated with the Seebeck effect does not grow in direct proportion with the temperature gradient, but could be affected by the temperature-dependent silicon doping profile and induced electron mobility in the conducting sample. In addition, the measured contact potential does not display evidence of a space charge effect. A high density of surface states supports the assumption that the work function differences and surface potential may be neglected in comparison to the effects of the changing tip bias and probe temperature.

CHAPTER 4

CONCLUSIONS AND FUTURE WORK

This work has described two applications of the heated silicon probe in materials characterization. The objective of the first experiment was to provide evidence of material phase transitions by local thermal analysis. This was achieved by heating the probe in contact with the substrate and subsequently analyzing its response. The second implemented the probe in a series of force-distance measurements to establish its potential use in scanning Kelvin probe microscopy. The aim was to quantify the influence of heat on the extracted contact potential between the semiconducting tip and a conducting sample. Both experiments rely on AFM feedback to quantify the force between tip and sample as a function of their separation distance.

In the first experiment, it was determined that the softening temperature of the substrate is sensitive to the applied contact force. In general, contact resistance decreased with force which augmented heat loss to the substrate and achieved earlier onset of the observed transitions. Thermal analysis of a polymer (HDPE) yielded multiple distinct transitions reflecting the changing surface area between tip and substrate during indent formation. Similar analysis was performed on a softer substrate (aspirin) and the tip was displaced at a relatively gradual rate with steady heat dissipation until the effects of reduced subsurface viscosity became likely. By comparing measured probe resistance with the tip height, this LTA method identifies an accurate temperature range in which the phase transition occurs. However, the results also suggest that interpretation of the softening point is dependent upon surface roughness and rigidity. Knowledge of the tip-sample interaction as a function of temperature and force is important for techniques

which rely on LTA to identify material phases by comparing the observed transitions to bulk values. The rate at which the probe is heated and cooled could be varied to better characterize the sample response in terms of the tip displacement per degree temperature change. Future work may therefore include increasing the voltage ramp rate or isothermally probing the surface at various temperatures within the expected transition range. Coupled with the varied contact force, this information could characterize factors which affect scanning mode measurements. For example, an isothermal study of a material response during indent formation could be compared against the depth-specific information obtained by frequency-modulated thermal probe microscopy. Quantifying the influence of contact force may also help to decouple signals related to material transitions and those dependent on the tip-sample interaction.

The heated Kelvin probe experiment indicates that the shift in contact potential increases with the applied temperature gradient. This was witnessed for all tip potentials, though the unbiased case was particularly used to illustrate the effect. The sign of the contact potential is mainly determined by the magnitude of the tip bias relative to the negative thermal voltage arising from the Seebeck effect. The silicon-gold work function difference and silicon surface potential also contribute to the contact potential, but are neglected when considering a change in the temperature gradient. Therefore, the fact that the magnitude of the offset declines with consecutively higher probe temperatures might suggest that there is an adverse effect on the field by applying too much heat. Thermally induced deflection is not assumed to be a factor since the cantilever was allowed to reach steady state prior to each experiment. However, the distribution of impurities in the tip and legs could change significantly with the temperature gradient, thus affecting the

thermal voltage and measured contact potential. This warrants heating the probe to higher temperatures to see if the trend persists.

Future work for the Kelvin probe experiment also includes varying the approach velocity during the force-distance measurement to determine whether it has any influence on the measured contact potential. A faster approach could affect heat dissipation to the substrate and the depth of propagation. Characterizing the tip-sample interaction through the contact potential might also enable in the design of a heated probe that could function separately as an electrode. This would allow the tip to characterize materials based on simultaneous measure of their thermal and electrical responses.

REFERENCES

1. Bhushar, B. and O. Marti, *Scanning Probe Microscopy - Principle of Operation, Instrumentation, and Probes*, in *Nanotribology and Nanomechanics*. 2005, Springer. p. 41-115.
2. Hammiche, A., et al., *Scanning Thermal Microscopy: Subsurface Imaging, Thermal Mapping of Polymer Blends, and Localized Calorimetry*. *Journal of Vacuum Science Technology B*, 1996. 14(2): p. 1486-1491.
3. Guillaumin, V., P. Schmutz, and G.S. Frankel, *Characterization of Corrosion Interfaces by the Scanning Kelvin Probe Force Microscopy Technique*. *Journal of the electrochemical society*, 2001. 148(5): p. B163-B173.
4. King, W.P., et al., *Design of Atomic Force Microscope Cantilevers for Combined Thermomechanical Writing and Thermal Reading in Array Operation*. *Journal of Microelectromechanical Systems*, 2002. 11(6).
5. Hammiche, A., et al., *Highly Localized Thermal, Mechanical, and Spectroscopic Characterization of Polymers using Miniaturized Thermal Probes*. *Journal of Vacuum Science Technology B*, 2000. 18(3): p. 1322.
6. Craig, D.Q.M., et al., *Pharmaceutical Applications of Microthermal Analysis*. *Journal of Pharmaceutical Sciences*, 2002. 91(5).
7. Royall, P.G., et al., *Identification of Crystalline and Amorphous Regions in Low Molecular Weight Materials using Microthermal Analysis*. *Journal of Physical Chemistry B*, 2001. 105(7021-7026).
8. Bond, L., et al., *Differential Scanning Calorimetry and Scanning Thermal Microscopy Analysis of Pharmaceutical Materials*. *International Journal of Pharmaceutics*, 2002. 243: p. 71-82.
9. Harding, L., M. Reading, and D.Q.M. Craig, *The Development of Heated Tip Force-Distance Measurements as a Novel Approach to Site-Specific Characterisation of Pharmaceutical Materials*. 2007.
10. B.A.Nelson and W.P. King, *Measuring Material Softening with Nanoscale Spatial Resolution using Heated Silicon Probes*. *Review of Scientific Instruments*, 2007. 78.
11. Price, D.M., et al., *Micro-thermal Analysis: Scanning Thermal Microscopy and Localized Thermal Analysis*. *International Journal of Pharmaceutics*, 1999. 192: p. 85-96.

12. Huey, B.D., D. Lisjak, and D.A. Bonnell, *Nanometer-Scale Variations in Interface Potential by Scanning Probe Microscopy*. Journal of the American Ceramic Society, 1999. 82(171): p. 1941-1944.
13. Schmutz, P. and G.S. Frankel, *Characterization of AA2024-T3 by Scanning Kelvin Probe Microscopy*. Journal of the Electrochemical Society, 1998. 145(7): p. 2285.
14. H.O.Jacobs and A.Stemmer, *Measuring and Modifying the Electric Surface Potential Distribution on a Nanometer Scale: a Powerful Tool in Science and Technology*. Surface and Interface Analysis, 1999. 27: p. 361-367.
15. Shi, L. and U.S. Ghoshal, *Method and Apparatus for Measuring Dopant Profile of a Semiconductor*. 2005, International Business Machines Corporation: US.
16. Bian, Z., et al., *Three-dimensional modeling of nanoscale Seebeck measurements by scanning thermoelectric microscopy*. Applied Physics Letters, 2005. 87.
17. Laio, C.N. and K.N. Tu, *Direct Measurement of Contact Potential using Seebeck Potential*. Journal of Applied Physics, 2002. 92(1): p. 635.
18. Lee, J., et al., *Electrical, Thermal, and Mechanical Characterization of Silicon Microcantilever Heaters*. Journal of Microelectromechanical Systems, 2006.
19. Chui, B.W., et al., *Intrinsic-Carrier Thermal Runaway in Silicon Microcantilevers*. Microscale Thermophysical Engineering, 1999: p. 217-228.
20. Beechem, T., et al., *Simultaneous Mapping of Temperature and Stress in Microdevices using Micro-Raman Spectroscopy*. Review of Scientific Instruments, 2007.
21. Hutter, J.L. and J. Bechhoefer, *Calibration of Atomic-Force microscope Tips*. Review of Scientific Instruments, 1993. 64(7): p. 1868-1873.
22. Pinnaduwege, L.A., et al., *Detection of Trinitrotoluene via Deflagration on a Microcantilever*. Journal of Applied Physics, 2004. 95(10).
23. Thundat, T., et al., *Thermal and Ambient-Induced Deflections of Scanning Force Microscope Cantilevers*. Applied Physics Letters, 1994. 64(21).
24. Butt, H.J., B. Capella, and M. Kappl, *Force Measurements with the Atomic Force Microscope: Technique, Interpretation, and Applications*. Surface Science Reports. 59(2005): p. 1-152.
25. Kasap, S., *Thermoelectric Effect in Metals: Thermocouples*, in *Principles of Electronic Materials and Devices (2nd edition)*. 2001, McGraw Hill.

26. Herwaarden, A.W.V., *The Seebeck Effect in Silicon ICs*. *Sensos and Actuators*, 1984. 6: p. 245-254.
27. Fritzsche, H., *A General Expression for the Thermoelectric Power*. *Solid State Communications*, 1971. 9: p. 1813-1815.
28. Muller, R.S. and T.I. Kamins, *Device Electronics for Integrated Circuits*. 1986.
29. Meyer, J.-P., et al., *Charge Transport in Thin Films of Molecular Semiconductors as Investigated by Measurements of Thermoelectric Power and Electrical Conductivity* *Thin Solid Films*, 1995. 258(1-2): p. 317-324.
30. Wu, Y., *Effect of Space Charges on Micro- to Nanoscale Electrostatic Actuation*. 2005, University of Illinois Urbana-Champaign.